NASA/CR-1998-206933

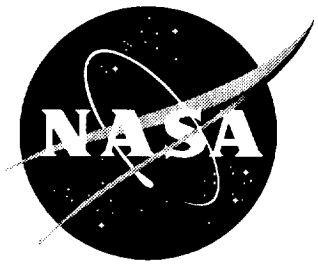

An Investigation of Candidate Sensor-Observable Wake Vortex Strength Parameters for the NASA Aircraft Vortex Spacing System (AVOSS)

Christopher Rhoads Tatnall
The George Washington University,
Joint Institute for Advancement of Flight Sciences,
Langley Research Center, Hampton, Virginia

National Aeronautics and
Space Administration

Langley Research Center
Hampton, Virginia 23681-2199

Prepared for Langley Research Center
under Cooperative Agreement NCC1-24

March 1998

Available from the following:

NASA Center for AeroSpace Information (CASI)
800 Elkridge Landing Road
Linthicum Heights, MD 21090-2934
(301) 621-0390

National Technical Information Service (NTIS)
5285 Port Royal Road
Springfield, VA 22161-2171
(703) 487-4650

ABSTRACT

The Aircraft Vortex Spacing System (AVOSS) under development at NASA is designed to prescribe safe and accurate aircraft landing approach separation distances. A key component of the AVOSS is a stationary ground sensor, making wake observations to verify predicted behavior. These readings would ensure safety by giving advanced warning of unexpectedly hazardous conditions. This task requires knowledge of a flowfield strength metric which gauges the severity of disturbance an encountering aircraft could potentially experience.

Several proposed strength metric concepts are defined and evaluated for various combinations of metric parameters and sensor line-of-sight elevation angles. Representative populations of generating and following aircraft types are selected, and their associated wake flowfields are modeled using various wake geometry definitions. All aircraft disturbance and metric calculations are performed applying two different methodologies in order to include results for all ranges of vortex intensity. Metric candidates are then rated and compared based on the correspondence of their computed values to associated aircraft response values, using basic statistical analyses.

ACKNOWLEDGMENTS

Some of the original concepts and information used in this study can be attributed to other individuals. Both the use of a dual-vortex flowfield for computations and the flat-plate roll moment metric were originally proposed by Dr. Roland Bowles, a consultant and retired NASA engineer. The velocity gradient metric concept was informally suggested by Eric Stewart, an engineer at NASA Langley. The representative following and generating aircraft with accompanying data were selected from a fairly comprehensive list of aircraft typically operating at US airports, compiled June 1995 by Robert Stuever, also an engineer at NASA Langley.

TABLE OF CONTENTS

LIST OF SYMBOLS

b	Aircraft Wing Span
$\bar{b}$	Vortex Pair Separation Distance
B	Plate Span
c , c_r	Aircraft Local, Root (Mid-Span) Wing Chord
C	Point About Which All Velocity Measurements Are Centered For a Given Metric
C_{l_α} , C_{L_α}	Aircraft Two-Dimensional, Three-Dimensional Wing Lift Curve Slopes
$C_{\ell_{ind}}$, $C_{L_{ind}}$	Total Vortex-Induced Roll Moment, Lift Coefficients for Entire Flowfield
C_{ℓ_C}	Aircraft Roll Control Input Coefficient, Assuming Maximum Control Input
$C_{\ell_{\bar{p}}}$	Aircraft Roll Damping Coefficient, Where Derivative is Taken With Respect to Non-Dimensional Roll Rate $\bar{p}=\left(\dot{\Phi}b\right)/(2V)$
C_{ℓ_V} , C_{L_V}	Vortex Induced Roll Moment, Lift Coefficients for Single Vortex
$\left(C_{\ell_V}\right)_{MAX}$	Maximum Possible Roll Moment Coefficient Induced on an Aircraft As It Encounters a Given Flowfield at the "Worst-Case" Position and Bank Angle
H_S	Flat-Plate Roll Moment
I_{XX}	Aircraft Mass-Moment-of-Inertia About the Roll Axis
k	Index Denoting a Metric's Order of Preference Relative to All Candidates
K	Total Number of Candidate Strength Metrics
L	Aircraft Lift
m	Aircraft Mass
N	Total Number of Pairs of Velocity Observations Used to Approximate Either Flat-Plate Average Circulation or Roll Moment
O	Point Indicating the Location of the Ground Sensor
P_i	Point At Which Velocity V_{LOS_i} is Observed
$\bar{q}$	Freestream Dynamic Pressure, $\frac{1}{2}\rho V^2$
r	Radial Coordinate From Point About Which Local/Average Circulation is
r_a , r_b	Inner, Outer Radial Limits Between Which Average Circulation is Determined
r_C	Vortex Core Radius
r_j	Radial Distance From Center Point C to j^{th} Pair of Velocity Observation Points $\left(P_i\right)_j$ For Approximation of Flat-Plate Average Circulation
r_{OC} , r_{OPi}	Distances Between Points O and C, Points O and P_i
s	Plate-Spanwise Coordinate Used in Computing Flat-Plate Roll Moment

s_j	Plate-Spanwise Distance From Center Point C to j^{th} Pair of Velocity Observation Points $(P_i)_j$ For Approximation of Flat-Plate Roll Moment
S	Aircraft Wing Area
S_k	Score Value Assigned to k^{th} Metric Based on Relative Performance
t	Time
T_P	Pilot Response Delay Time
V	Aircraft Velocity
V_{LOS}	Observed Line-of-Sight Velocity
w_{NP}	Induced Velocity Component Normal to Plate
w_T	Induced Tangential Velocity With Respect to Vortex Center
w_Y, w_Z, w_ζ	Induced Velocity Components in the Y-, Z- and ζ-Directions
W	Aircraft Weight
(Y , Z)	Inertial Coordinates
α_i	Vortex Induced Angle of Attack
δr , δs	Incremental Distance Between Velocity Observation Points $(P_i)_j$ With Flat-Plate Average Circulation, Roll Moment Metrics
ΔR	Distance Separating Velocity Observation Points P_i Used to Approximate Velocity Gradient
ΔV_{LOS}	Difference in Observed Velocities V_{LOS_i} Used to Approximate Velocity Gradient
Φ	Aircraft Roll Angle
Φ_{MAX}	Maximum Aircraft Roll Disturbance Angle Experienced During a Wake Vortex Encounter
Γ (r)	Local Circulation at a Given Radius r
Γ_∞	Total Vortex Circulation (Γ (r) , $r \rightarrow \infty$)
Γ_{BH} (r) , Γ_L (r)	Local Vortex Circulation Based on Burnham-Hallock, Lamb Vortex Models
Γ_V (r)	Local Circulation of a Single Vortex at a Given Radius r From Its Center
$\overline{\Gamma}, \hat{\Gamma}$	True, Observed ("Flat-Plate") Average Circulations
λ , λ_F	Taper Ratios of Flat Plate, Following Aircraft's Wing
θ	Sensor Center Line-of-Sight Elevation Angle, Measured From Ground Level
ρ	Ambient Air Density
σ_j	Sweep Angle of Sensor Line-of-Sight Associated With j^{th} Pair of Velocity Observation Points $(P_i)_j$, Measured From Center Line-of-Sight r_{OC}
(η, ζ)	Aircraft Body-Fixed Coordinates

Subscripts

F	Refers to Wake-Encountering (Following) Aircraft
G	Refers to Wake-Generating (Leading) Aircraft
i	Index Specifying Individual Velocity Observation in a Given Pair ($i = 1 , 2$)
j	Index Specifying Pair of Velocity Observations in Total Number of Pairs Used to Approximate Flat-Plate Average Circulation or Roll Moment ($j = 1 , 2 , 3 , \ldots N$)
LV, RV	Denotes Positions of Left, Right Vortices in a Pair

rel	Denotes Position/Distance Specified Relative to the Vortex Center
V	Refers to a Single Vortex

Abbreviations

2-D	Two-Dimensional
ATC	Air Traffic Control
AVOSS	Aircraft Vortex Spacing System
IFR	Instrument Flight Rules
NASA	National Aeronautics & Space Administration
TAP	Terminal Area Productivity
UK	United Kingdom
US	United States

LIST OF FIGURES

1. INTRODUCTION

The counter-rotating pair of wake vortices shed by flying aircraft can pose a serious threat to ensuing aircraft, particularly on landing approach as aircraft are likely to be aligned with the freshly-generated vortices from the previous aircraft. To allow adequate time for the vortices to disperse/decay, landing aircraft are required to maintain certain fixed separation distances. Aircraft are categorized according to their rated maximum takeoff weights, and separation distances are prescribed based on the weight classifications of the leading and following aircraft in a pair. Air Traffic Control (ATC) procedures in the US provide two modes of operation: the spacing standards shown in Table 1 are applied when ATC is responsible for aircraft separation under instrument flight rule (IFR) conditions. The pilot is responsible for maintaining adequate separation when visual approach procedures are in effect. A similar four-class system is used in the UK, although it is enforced in all visibility conditions and contains generally larger separation values [Vicroy et al. 1994].

TABLE 1

CURRENT U.S. WAKE VORTEX AIRCRAFT SEPARATION STANDARDS IN NAUTICAL MILES. AIRCRAFT CLASSIFICATION BASED ON RATED MAXIMUM TAKEOFF WEIGHTS [U.S. Dept. of Transportation 1997, 5-5-2, A-1].

Following Aircraft	Leading Aircraft			
	Heavy	Boeing 757	Large	Small
Heavy	4	4	2.5*	2.5*
Large	5	4	2.5*	2.5*
Small	6	5	4	2.5*
(* For runway occupancy time ≤ 50 seconds; otherwise 3 nm)				
Class partitions (revised August 1996):				
Heavy	Large			Small
> 255,000 lb.	≦ 255,000 lb. and > 41,000 lb.			≦ 41,000 lb.

Lacking sufficient understanding and means of monitoring vortex behavior, these standards consist of fixed values resulting from conservative empirical estimates based on experimental results and pilot experiences. This heuristic approach compromises safety and restricts airport capacity. Numerous wake vortex incidents have been reported in both the US and UK, many while adhering to prescribed separations [Johnson 1991; Critchley and Foot 1991], due to unexpectedly hazardous conditions not accounted for by limited past observations. However, in most situations the separation constraints are too extreme and restrict airport capacity, since the strong meteorological effects on wake motion and decay are not considered. Safety requires the fixed separation values must accommodate the perceived "worst-case" scenario, the most dangerous aircraft pairing in a given leader/follower class combination flying in conditions (local atmosphere, terrain) which are least effective in dispersing the vortices. Although slight improvements in safety and efficiency can be attained by adjusting the choice of classification parameter and class partition values [Tatnall 1995], these disadvantages are inevitable with fixed separation criteria.

With air traffic growth far exceeding the number of new facilities, an increasing number of US airports are becoming capacity-saturated. In response, NASA is conducting research through the Terminal Area Productivity (TAP) Program to optimize various stages of airport operations [Vicroy et al 1994]. One of the program's four primary objectives is safely reducing aircraft separation constraints; early studies estimate that this improvement by itself could yield a 10-15% jump in capacity [Scott 1993, 69-76]. The Aircraft Vortex Spacing System (AVOSS) under development within the TAP Program will significantly improve spacing accuracy by adjusting separation values based on observations of meteorological and wake conditions. The AVOSS conceptual framework consists of three main elements: a meteorological subsystem providing atmospheric information based on both current input and short-term forecasting; a

predictor subsystem which decides the appropriate spacing based on weather, airport, and aircraft-specific factors; a sensor subsystem to monitor the actual vortices' strength and position, providing feedback to the predictor [Hinton 1995, 4]. Sensor readings would also ensure safety by allowing adequate notice to abort a landing in case of unexpectedly strong wakes. This capability depends on knowledge of some wake-flowfield parameter, a "strength metric", which quantifies the threat posed to an approaching aircraft.

This project is a continuation of research to define a sensor-observable flowfield parameter that robustly predicts the transient dynamic response an aircraft would experience while encountering the given flowfield. Three metric concepts are considered, all of which are based on flowfield measurements taken by an idealized, line-of-sight velocity sensor: a velocity gradient, an estimated average circulation, and a parameter simulating the roll moment exerted on a flat plate. The main objective of this research is to evaluate different variations of these basic models with regard to their ability to predict aircraft disturbance. Although there is not yet a universally accepted definition of "aircraft disturbance" for these purposes, in this research it will be quantified as the maximum bank angle a following aircraft would experience in a given vortex flowfield, Φ_{MAX}.

The following sections outline the models and assumptions used to determine aircraft disturbance and corresponding strength metric values. Data are then produced for a variety of conditions, and the individual metrics are compared using statistical analyses.

2. DESCRIPTION OF MODELS

Assuming a simple dual-vortex flowfield, analytical expressions are developed for vortex-induced aircraft loads and the three candidate sensor-observable strength metrics. These expressions are linear in terms of flowfield velocity and thus their aggregate results for a multi-vortex system can be determined by superimposing the effects of each individual vortex. Therefore, derivations of these models correspond to a single vortex with positive circulation. In contrast, the non-linear aircraft dynamic response model is based on the complete flowfield, thus requiring total values of induced lift and roll moment in its evaluation.

Wake Vortex Flowfield

In flight test observations, vortices appear to consist of a slender core of laminar flow, encased in a slower-moving turbulent layer. The vortices are subject to transport by mutually-imposed downwash and ambient winds, frequently causing the pair to tilt as they descend unevenly. Eventually, the vortices either become unstable through a variety of processes or gradually decay due to viscous effects, depending on surrounding conditions [Hallock 1991, 13-16].

The simplified flowfield model used in this research consists of a stationary pair of 2-D, axisymmetric vortices, neglecting atmospheric and ground effects. The Burnham-Hallock [Burnham and Hallock 1982] and Lamb [Saffman 1992, 253; see also Lamb 1932] vortex circulation models are used, both of which are smooth and continuous profiles. They are, respectively,

$$\Gamma_{BH}(r) = \Gamma_{\infty}\left(\frac{r^2}{r^2 + {r_C}^2}\right) \tag{1}$$

$$\Gamma_{L}(r) = \Gamma_{\infty}\left(1 - e^{\left(-r^2/{r_C}^2\right)}\right) \tag{2}$$

where Γ_{∞} is total circulation, r is radial distance from the vortex center, and r_C is the core radius. Assuming the spanwise lift distribution of the leading aircraft is elliptical, Prandtl's lifting line theory

estimates that the turbulent wake shed from the wing will eventually roll up into two parallel counter-rotating vortices separated by a distance $\bar{b} = (\pi/4)b_G$, each having total circulation

$$\Gamma_\infty = \frac{L_G}{V_G\left(\pi/4\right)b_G\rho} \tag{3}$$

[Karamcheti 1980, 550] where L_G ,V_G and b_G are the lift, velocity and wing span of the generating aircraft, respectively, and ρ is ambient air density. Because the generating aircraft is assumed to be in steady-level flight, its weight W_G is substituted for lift.

Here, vortex decay is represented by a uniform decrease in the total circulation, with no change in vortex position or circulation profile. In previous work using similar models and assumptions, decreasing circulation strength was obtained using a conservative linear decay law, which in its simplest form is expressed

$$\frac{\Gamma_\infty(t)}{\Gamma_\infty(0)} = 1 - \frac{4W_G}{\pi^4\,\rho V_G\,{b_G}^3}\,t \tag{4}$$

[Tatnall 1995, 29-32].

Aircraft Roll Response

In computing the vortex induced loads during an encounter, the following aircraft is modeled as a flat (i.e. without dihedral or twist), linearly-tapered wing which extends to the aircraft centerline; fuselage, nacelles and tail surfaces are excluded (see Figure 1). The dynamic model allows the aircraft to roll and translate vertically and laterally, in response to the vortex induced lift and roll moment, roll damping and pilot input. For purposes of response calculations, the inertial coordinate system is assumed to have a downward-pointed Z-axis in keeping with aircraft stability and control conventions. As will be later noted, this is reversed for all metric calculations in keeping with metric and sensor conventions.

Vortex Induced Aircraft Loads

By definition of circulation for an axisymmetric vortex, $\Gamma_V(r)$, the tangential velocity at some distance r from the center is

$$w_{T_V}(r) = \Gamma_V(r)/2\pi r \tag{5}$$

The flowfield velocity components at a fixed location (Y,Z) induced by a vortex centered at (Y_V, Z_V) can be expressed in terms of relative coordinates $(Y_{rel}, Z_{rel}) = (Y - Y_V, Z - Z_V)$:

$$\begin{Bmatrix} w_{Y_V}(Y_{rel}, Z_{rel}) \\ w_{Z_V}(Y_{rel}, Z_{rel}) \end{Bmatrix} = w_{T_V}(r_{rel}) \cdot \begin{Bmatrix} -Z_{rel}/r_{rel} \\ Y_{rel}/r_{rel} \end{Bmatrix} \tag{6}$$

where $r_{rel} = \sqrt{{Y_{rel}}^2 + {Z_{rel}}^2}$.

The induced aircraft load models are based on strip theory [Von Mises, 1959], requiring induced velocity to be expressed in aircraft body-fixed coordinates (η,ζ), as shown in Figure 1. The position coordinates are transformed by substituting

$$\begin{Bmatrix} Y_{rel} \\ Z_{rel} \end{Bmatrix} = \begin{Bmatrix} Y_F - Y_V \\ Z_F - Z_V \end{Bmatrix} + \begin{bmatrix} \cos\Phi_F & -\sin\Phi_F \\ \sin\Phi_F & \cos\Phi_F \end{bmatrix} \begin{Bmatrix} \eta \\ \zeta \end{Bmatrix} \tag{7}$$

into Eq. (6), where (Y_F, Z_F) is the follower's position in inertial coordinates and Φ_F is roll angle. The flat-wing assumption allows further simplification by setting $\zeta = 0$. The velocity component normal to the wing is then found using

$$w_{\zeta_V} = -w_{Y_V} \sin\Phi_F + w_{Z_V} \cos\Phi_F \tag{8}$$

The small angle approximation $\alpha_i = -w_{\zeta_V} / V_F$ is used for the local induced angle-of-attack, where V_F is the follower's airspeed. Finally, analytical expressions for the induced loads are obtained, integrating the lift and roll moment induced at each differential "strip" along the wing:

$$\begin{aligned} C_{L_V}(Y_F, Z_F, \Phi_F) &= \frac{\int_{-b_F/2}^{b_F/2} \left\{ C_{l_\alpha F} \cdot \alpha_i(Y_F, Z_F, \Phi_F, \eta) \cdot c_F(\eta) \cdot \bar{q} \right\} d\eta}{\bar{q} \cdot S_F} \\ &= \frac{C_{L_\alpha F} \cdot c_{r_F}}{S_F} \int_{-b_F/2}^{b_F/2} \left\{ \left(1 - \frac{(1-\lambda_F)}{b_F/2} |\eta| \right) \cdot \alpha_i(Y_F, Z_F, \Phi_F, \eta) \right\} d\eta \end{aligned} \tag{9}$$

and

$$\begin{aligned} C_{\ell_V}(Y_F, Z_F, \Phi_F) &= -\frac{\int_{-b_F/2}^{b_F/2} \left\{ C_{l_\alpha F} \cdot \alpha_i(Y_F, Z_F, \Phi_F, \eta) \cdot c_F(\eta) \cdot \bar{q} \cdot \eta \right\} d\eta}{\bar{q} \cdot S_F \cdot b_F} \\ &= -\frac{C_{L_\alpha F} \cdot c_{r_F}}{S_F \cdot b_F} \int_{-b_F/2}^{b_F/2} \left\{ \left(1 - \frac{(1-\lambda_F)}{b_F/2} |\eta| \right) \cdot \alpha_i(Y_F, Z_F, \Phi_F, \eta) \cdot \eta \right\} d\eta \end{aligned} \tag{10}$$

in which $C_{L_\alpha F}, c_F, c_{r_F}, b_F, S_F$ and λ_F are respectively the lift-curve slope, local chord, root (centerline) chord, span, area and taper ratio of the following aircraft's wing, and $\bar{q}$ is the dynamic pressure. The negative sign compensates for the fact that a positive angle of attack (positive lift) acting through a positive moment arm (starboard wing) produces a negative roll moment with the given sign conventions.

Dynamic Model

The aircraft can roll and translate laterally and vertically in response to the induced lift and roll moment. The equations of motion are

$$
\begin{aligned}
m_F \ddot{Y}_F &= \left(W_F + \bar{q}\, S_F\, C_{L_{ind}}\right) \sin \Phi_F \\
m_F \ddot{Z}_F &= W_F - \left(W_F + \bar{q}\, S_F\, C_{L_{ind}}\right) \cos \Phi_F \\
I_{XX_F}\, \ddot{\Phi}_F &= \bar{q}\, S_F\, b_F \left[\left(\frac{b_F\, \dot{\Phi}_F}{2 V_F} \right) C_{\ell_{\bar{p}} F} + C_{\ell_{ind}} - \mathcal{H}\left(t - T_P\right) \frac{\Phi_F}{|\Phi_F|} C_{\ell_C F} \right]
\end{aligned}
\qquad (11)
$$

where $m_F, W_F, I_{XX_F}, C_{\ell_{\bar{p}} F}$ and $C_{\ell_C F}$ are respectively the mass, weight, rolling axis mass-moment-of-inertia, roll damping coefficient and full-input roll control coefficient of the following aircraft. The non-linear dynamic system must be solved numerically, at each step using the complete-flowfield values for vortex induced lift and roll moment coefficient, $C_{L_{ind}}$ and $C_{\ell_{ind}}$. These terms are simply the sums of the respective induced lift and roll moment coefficients for individual vortices (Eqs. (9) and (10)), and therefore must be re-computed at each integration step since they are dependent on Y_F, Z_F and Φ_F. The step-function used in the control input term, $\mathcal{H}\left(t - T_P\right)$, accounts for the pilot reaction time, after which full roll-control authority is applied to level the wing. In all cases, the suggested delay of T_P = 0.6 seconds is used [Tinling 1977, 11-22].

The following aircraft is assumed to encounter the wake in wings-level flight on a standard glideslope of 3 degrees. The position at which the aircraft initially penetrates the wake is determined such that the greatest encounter roll perturbation is experienced in the given flowfield conditions. Due to the non-linearity of the dynamic model, these coordinates cannot be analytically determined, and the computational cost of the required numerical integration makes a Monte-Carlo approach impractical. An acceptable alternative used in previous research is to insert the aircraft at the location of greatest induced roll moment [Tatnall 1995]. For limited validation of this assumption, values of induced roll moment and maximum bank angle deviations are computed for three different aircraft pairs as the follower's initial position is varied laterally with respect to the midpoint of the vortex pair. As shown in Figure 2, the initial follower locations corresponding to the greatest values of aircraft disturbance and highest initial roll moment show excellent agreement for all three aircraft pairs. Thus, the initial values for Eqs. (11) used in all cases are

$$
\left[
\begin{array}{ll}
Y_F = Y_F @ \left(C_{\ell_W}\right)_{MAX} & \dot{Y}_F = 0 \\
Z_F = Z_F @ \left(C_{\ell_W}\right)_{MAX} & \dot{Z}_F = V_F \tan 3^\circ \\
\Phi_F = 0 & \dot{\Phi}_F = 0
\end{array}
\right]_{t=0}
\qquad (12)
$$

Candidate Flowfield Strength Metrics

The three types of parameters for assessing potential aircraft disturbance in a given flowfield are all based on a series of discrete line-of-sight velocity measurements taken by a stationary ground sensor. Velocities oriented away from the sensor are considered positive, and sensor-specific limitations are neglected. Also, the inertial coordinate system used for all metric calculations is oriented such that the Z-axis is directed upward. This discrepancy in the coordinate systems used for aircraft response and metric values is

insignificant since the intent is to relate the *magnitudes* of each. With this axis system, positive circulation is counter-clockwise.

Velocity Gradient

This metric model is based on the line-of-sight velocity gradient at a point *C*, approximated over the length ΔR, as shown in Figure 3. In order to locate the observation points, their polar coordinates relative to the ground sensor are first determined:

$$r_{OC} = \sqrt{(Y_C - Y_O)^2 + (Z_C - Z_O)^2} \; ; \; \theta = tan^{-1}\left(\frac{Z_C - Z_O}{Y_C - Y_O}\right) \qquad (13)$$

so the distances from the ground sensor to the measurement points are $r_{OP_1} = r_{OC} - \Delta R/2$ and $r_{OP_2} = r_{OC} + \Delta R/2$. Transforming back to Cartesian coordinates, the observation points are located at $\left(Y_{P_i}, Z_{P_i}\right) = \left(Y_O + r_{OP_i}\, cos\theta, Z_O + r_{OP_i}\, sin\theta\right) \;\; i = 1,2.$

The velocity components at each point, $\left(w_{Y_V i}, w_{Z_V i}\right)$ $i = 1,2$, induced by a vortex at $\left(Y_V, Z_V\right)$ such that $\left(Y_{rel_i}, Z_{rel_i}\right) = \left(Y_{P_i} - Y_V, Z_{P_i} - Z_V\right)$ and $r_{rel_i} = \sqrt{{Y_{rel_i}}^2 + {Z_{rel_i}}^2}$ $i = 1,2$, can be computed using Eqs. (5) and (6). Finally, the observed line-of-sight velocities $V_{LOS_i} = w_{Y_V i} \cos\theta + w_{Z_V i} \sin\theta \;\; i = 1,2$, are used to calculate the gradient metric:

$$\frac{\Delta V_{LOS}}{\Delta R} = \frac{V_{LOS_2} - V_{LOS_1}}{\Delta R} \qquad (14)$$

"Flat-Plate" Average Circulation

The principle of this metric is to estimate the average of the velocity circulation values around a given center point *C* between the radial limits r_a and r_b, based on a series of pairs of discrete tangential velocity observations. The definition of average circulation is given as:

$$\overline{\Gamma}_{r_a, r_b} = \frac{\int_{r_a}^{r_b} \Gamma(r)\, dr}{r_b - r_a} \qquad (15)$$

where $\Gamma(r)$ is the local circulation at radius *r*. However, actual circulation can only be determined with complete knowledge of the 2-D velocity flowfield in the given region, which is impossible to obtain with a stationary line-of-sight sensor. Therefore, an alternative method is used wherein the circulation at a given radius is approximated as the mean of the observed tangential velocities. In this manner, the integral in Eq. (15) can be solved numerically using the discrete pairs of velocity observations to estimate the local circulations at each of *N* discrete radii. This flowfield parameter is distinguished as "flat-plate" average circulation because it resembles the effect of measuring the velocities traversing an imaginary plate. As shown in Figure 4, a fixed sensor cannot actually measure tangential velocities crossing a flat plate located some finite distance away. As the sensor's sweep angle σ_j increases for each tangential velocity measurement, the observation points diverge from the flat plate, forming an elliptical arc instead.

Again, r_{OC} and θ can be found using Eq. (13). For each step in the integration of (15), the coordinates of the observation points $(P_1)_j$ and $(P_2)_j$ are

$$\left(Y_{P_i}, Z_{P_i}\right)_j = \left(Y_O + \left(r_{OP_i}\right)_j cos\left(\theta \mp \sigma_j\right), Z_O + \left(r_{OP_i}\right)_j sin\left(\theta \mp \sigma_j\right)\right) \quad i = 1,2 \qquad (16)$$

where $\left(r_{OP_i}\right)_j = \sqrt{{r_{OC}}^2 - {r_j}^2}$ and $\sigma_j = \tan^{-1}\left(r_j / \left(r_{OP_i}\right)_j\right)$ $i = 1,2$. The observed velocities $\left(V_{LOS_i}\right)_j$ $i = 1,2$ at each step are again found using relative vortex-relative coordinates with Eqs. (5) and (6), and transforming from inertial coordinates using

$$\left(V_{LOS_i}\right)_j = \left(w_{Y_V i}\right)_j \cos\left(\theta \mp \sigma_j\right) + \left(w_{Z_V i}\right)_j \sin\left(\theta \mp \sigma_j\right) \quad i = 1,2 \qquad (17)$$

Finally, these velocities computed at each step j can be combined to determine the flat-plate average circulation:

$$\hat{\Gamma}_{r_a, r_b} = \frac{\sum_{j=1}^{N}\left[\left(\left(V_{LOS_1}\right)_j - \left(V_{LOS_2}\right)_j\right)\pi r_j \, \delta r\right]}{r_b - r_a} \qquad (18)$$

where $\delta r = \left(r_b - r_a\right)/(N-1)$ is the radial stepsize used in the numerical integration, and the subtraction of line-of-sight velocities accounts for a negative value of V_{LOS_2} (i.e. towards the sensor) contributing to a positive value of circulation, as shown in Figure 4.

"Flat-Plate" Roll Moment

This metric, also previously studied [Hinton and Tatnall 1997], resembles the integral expression for induced roll moment given in Eq. (10). The model assumes a flat plate centered at point C with span B and taper ratio λ, and is oriented directly facing the sensor (i.e. normal to r_{OC}). This generic roll moment parameter which neglects all other aircraft-specific factors (airspeed, lift-curve slope, etc.), is given by the integral:

$$H_S = \int_{-B/2}^{B/2}\left(1 - \frac{(1-\lambda)}{B/2}|s|\right) \cdot w_{NP}(s) \cdot s \cdot ds \qquad (19)$$

where the s is the spanwise coordinate and w_{NP} is the local velocity normal to the plate at a given location. Similar to the average flat-plate circulation metric, the integral is solved numerically based on pairs of tangential velocity observations which represent velocities normal to the plate (see Figure 5). The procedure for determining these values are identical to the steps used in the circulation metric. The roll moment parameter can be simplified to:

$$H_S = \sum_{j=1}^{N}\left[\left(1 - \frac{(1-\lambda)}{B/2}|s_j|\right) \cdot \left(\left(V_{LOS_1}\right)_j - \left(V_{LOS_2}\right)_j\right) \cdot |s_j| \cdot \delta s\right] \qquad (20)$$

where s_j is the spanwise distance from C in either direction for the j^{th} step, $\delta s = (B/2)/(N-1)$ is the stepsize, and the subtraction accounts for negative values of V_{LOS_2} (i.e. towards sensor) contributing to positive values for roll moment (see Figure 5).

3. ANALYSIS

Using a representative aircraft population, induced bank angle data are generated for numerous flowfield conditions based on the assumptions and methods previously outlined. Strength metric data are also computed for each of the corresponding wakes, using variations of the three basic metric models. Simple statistical techniques are then applied to determine correlation between aircraft roll disturbance and metric data, allowing the candidate metrics to be quantitatively rated and compared.

Aircraft Response Calculations

To account for unpredictable or variable wake characteristics, all aircraft response and metric calculations are repeated for a variety of conditions. To keep the amount of data manageable, the representative lists of leading and following aircraft were each narrowed to 10, as given in Tables 2 and 3, respectively. The selection criteria were:

- Generally uniform coverage of the weight categories, with the leading aircraft list biased towards the heavier models and follower list biased towards the smaller ones, excluding general aviation aircraft
- Fair representation of the different aircraft manufacturers
- Inclusion of aircraft of particular interest, such as the Boeing 747-400 which is presently the heaviest in the US commercial fleet, and the Boeing 757-200 which has been the subject of past controversy due to its "high-lift" landing capabilities supposedly generating unusually hazardous wakes.

In all cases, the basic flowfield structure is a symmetrical pair of vortices located on either side of the origin $\left((Y_V, Z_V) = \left(\pm \bar{b}/2 \ , \ 0\right)\right)$. Aircraft response calculations for all leader/follower pairs from the lists are repeated for 12 combinations of flowfield parameters: both the Lamb and Burnham-Hallock profiles are used with 3 different core-radii (r_C = 2%, 4% and 6% of b_G) and 2 vortex separation distances ($\bar{b} = (\pi/4)b_G$ and $(3\pi/8)b_G$). Total circulation is determined using Eqs. (3) and (4), where vortex decay time is found by assuming a constant aircraft separation distance of 3 nm and converting to time using the generator's velocity only, V_G. In some operational scenarios, the actual distance-to-time conversion may also depend on the follower's velocity, V_F [Tatnall 1995, 44]. However, modeling the flowfield exclusively based on the characteristics of the generating aircraft yields acceptable results, and greatly reduces the amount of metric data since there are only 10 unique strengths $\left(\Gamma_\infty\right)$ for each of the 12 cases previously mentioned.

In previous research, a linear relationship between strength metric and aircraft roll-disturbance values, computed based on a flowfields of fixed strengths, did not show good correlation with wakes that were half as strong [Hinton and Tatnall 1997, 15]. Although this inconsistency can be attributed to non-linearity in the aircraft response model, it also raises the issue that a given strength metric may only correlate well to aircraft response in a certain range of flowfield strength. Therefore, additional calculations are made in which wake strength is based on a constant follower roll response of 10 degrees for all aircraft pairs, rather than a fixed separation distance. With no analytical solution for the maximum encounter roll disturbance, the vortex strength required for each aircraft pair must be found numerically. Also, now that the flowfield is a result of both generator and follower, metric values will have to be computed for all aircraft pair combinations.

TABLE 2

LIST OF LEADING (WAKE-GENERATING) AIRCRAFT STUDIED, WITH PERTINENT DATA.

	Name	Rated Max. Takeoff Wt. (kgf)	Rated Max. Landing Wt. (kgf)	Wing Span (m)	Approach Velocity (m/s)
1	Boeing 747-400	385,554	285,763	64.31	79
2	Boeing 777-200	267,619	201,849	60.94	71
3	Lockheed L1011-500	224,982	166,922	47.34	77
4	Airbus A330	212,009	173,998	59.56	70
5	McD DC-10-10	206,385	164,881	47.34	66
6	Boeing 767-200ER	156,489	129,274	47.58	72
7	Boeing 757-200	104,326	95,254	37.95	70
8	Boeing 727-200	86,409	70,080	32.92	69
9	McD DC-9-50	54,885	49,895	28.47	68
10	Gulfstream IV	31,615	26,535	23.47	67

TABLE 3

LIST OF FOLLOWING (WAKE-ENCOUNTERING) AIRCRAFT STUDIED, WITH PERTINENT DATA.

	Name	Rated Max. Takeoff Wt. (kgf)	Rated Max. Landing Wt. (kgf)	I_{xx} for Max. Landing Wt. ($kg\text{-}m^2$)	Wing				Approach Velocity (m/s)	Roll Damping Coeff.	(Full-Input) Roll Control Coeff.
					Span (m)	Area (m^2)	λ	$C_{L\alpha}$ (rad^{-1})			
1	McD DC-10-10	206,385	164,881	10,846,544	47.34	358.7	0.30	4.70	66	-0.407	0.062
2	Boeing 767-200ER	156,489	129,274	6,394,037	47.58	283.4	0.27	4.98	72	-0.447	0.051
3	Boeing 757-200	104,326	95,254	4,314,213	37.95	181.3	0.23	4.97	70	-0.462	0.060
4	Airbus A320-200	73,482	64,501	1,491,400	33.92	122.4	0.25	5.14	69	-0.512	0.040
5	Boeing 727-100	64,410	62,369	1,038,557	32.92	157.9	0.30	4.81	64	-0.451	0.029
6	Boeing 737-200	52,390	46,720	585,713	28.35	102.0	0.34	4.96	66	-0.498	0.030
7	DHC-8 Dash 8	18,643	18,144	203,373	27.43	56.2	0.48	5.43	51	-0.650	0.068
8	Learjet 35a	8,301	6,940	22,642	12.04	23.5	0.56	4.69	64	-0.440	0.020
9	BAe Super31	6,940	6,577	42,030	15.85	25.2	0.38	5.19	58	-0.560	0.034
10	Fairchild SA-227 Metro	6,577	6,350	39,319	17.37	28.7	0.33	5.24	58	-0.554	0.032

Strength Metric Calculations

The complete list of 24 candidate metrics, shown in Table 4, is comprised of variations on the 3 basic metric models outlined in the previous section. The metric names are assigned such that gradient, circulation, and roll moment metrics begin with the letters "D", "C", and "H" respectively, and denote the key properties of each specific metric (see Table 4). The values used for ΔR and B appear haphazard because the original computations were performed in British units, in which these lengths were chosen as uniform multiples of feet.

TABLE 4

SPECIFIC STRENGTH METRIC CANDIDATES WITH ASSOCIATED PROPERTIES.

$\Delta V_{LOS}/\Delta R$			$\hat{\Gamma}_{r_a, r_b}$			H_S		
Name	ΔR (m)	Y_C	Name	r_a (m)	r_b (m)	Name	B (m)	λ
D12L2	12.19	0.2 Y_{LV}	C5-10	5	10	H15tr0.3	15.24	0.3
D15L2	15.24	0.2 Y_{LV}	C10-15	10	15	H30tr0.3	30.48	0.3
D18L2	18.29	0.2 Y_{LV}	C7-15	7	15	H46tr0.3	45.72	0.3
D21L2	21.34	0.2 Y_{LV}	C5-15	5	15	H61tr0.3	60.96	0.3
D12L8	12.19	0.8 Y_{LV}	C1-5	1	5	H15tr0.7	15.24	0.7
D15L8	15.24	0.8 Y_{LV}	C1-10	1	10	H30tr0.7	30.48	0.7
D18L8	18.29	0.8 Y_{LV}	C3-10	3	10	H46tr0.7	45.72	0.7
D21L8	21.34	0.8 Y_{LV}	C1-15	1	15	H61tr0.7	60.96	0.7
Naming Conventions:								
D {ΔR*} L { 10 (Y_C/Y_{LV}) }			C {r_a} - {r_b}			H {B*} tr {λ}		
* Rounded to the Nearest Meter								

The velocity gradient metrics include gradients taken at 2 locations between the origin and left vortex, using 4 different values for ΔR at each of 12.19, 15.24, 18.29, and 21.34 m (40, 50, 60, 70 feet). Since the velocity gradient is intrinsically zero at either vortex or at the vortex-pair midpoint in the given symmetric flowfield, readings are instead arbitrarily centered about points 20% and 80% of the distance from the origin to the left vortex to obtain non-trivial solutions. In contrast, all flat-plate average circulation and roll moment metric readings are centered on the left vortex. In terms of the average circulation metrics, the same 8 combinations of radial limits (r_a, r_b) studied in the preceding work [Hinton and Tatnall 1997, Table 3] are used here. The roll moment metrics include combinations of the 4 plate spans 15.24, 30.48, 45.72, and 60.96 m (50, 100, 150, 200 feet) and the 2 taper ratios 0.3 and 0.7, which are intended to represent those characteristics of the selected following aircraft population.

It was found empirically that, under the given conditions, 50 pairs of velocity measurements are sufficient in numerically integrating any of the flat-plate metrics. For all metrics, the distance between the ground sensor and the center observation point is assumed to be r_{GC} = 304.8 m (1000 feet). Calculations are performed for both θ = 30 degrees and θ = 70 degrees, since the apparent strength of a vortex pair varies with viewing elevation angle.

Metric Quality Evaluation

The ability of each metric to predict aircraft roll response is quantified using one of two parameters, depending on which method is used to generate the data (see Figure 6). In the first approach, where aircraft disturbances are computed based on a constant 3 nm separation, each candidate is rated based on the quality of linear fit between its values and corresponding aircraft disturbance values. This is established using the Coefficient of Determination, whose values range from unity for an exact linear correlation, to zero for cases in which there is no relationship between given data sets [Scheaffer and McClave 1986, 341-369]. To account for the fact that the absence of wake should result in aircraft disturbance and metric values of zero, this data point is included in all linear regressions, although the line fit is not forced to intercept the origin as this yields questionable values for the Coefficient of Determination.

However, this methodology is not applicable with the second method which is based on fixed aircraft roll response values of 10 degrees for all cases. Instead, metric quality is assessed by the amount of scatter in a given set of metric values, based on the principle that a good metric should give consistent readings for the same value of aircraft bank angle. This is determined using standard deviation, normalized by the absolute value of the mean to facilitate comparison of different metric types.

Statistical analyses are repeated for 3 different "cuts" of the data: analyses are performed on all data for each of the two methodologies, so that there are a total of 2400 data points in each set; separate analyses are performed for each combination of the 10 following aircraft and the 12 wake geometry descriptions, so that there are 120 individual subsets each containing 20 data points; analyses are performed for each following aircraft in all wake conditions, so that there are 10 subsets each with 240 data points.

Because the ultimate objective is to rate the *relative* worth of the various strength metrics, each metric is assigned a "score" based on its position in a list of metrics sorted in order of preference (either descending order of Coefficient of Determination, or ascending order of Normalized Standard Deviation). A simple method for scoring the candidates is to assign values between unity and zero which linearly decrease in magnitude with decreasing order of preference. This metric score parameter is:

$$S_k = 1 - \frac{(k-1)}{K} \tag{21}$$

in which K is the total number under consideration and k is the sorted order of each individual. This parameter is useful where separate analyses are performed on individual subsets of data and the results averaged. Averaging the scores from each analysis gives insight on how consistently a given metric performed, rather than drawing conclusions simply based on the final mean values for each metric.

4. RESULTS AND DISCUSSION

With raw aircraft response and metric data produced using the models and constraints previously described, statistical analyses are applied to different groupings based on combinations of following aircraft and flowfield geometry conditions. Also, trends are studied between geometric properties of the most successful metrics and associated followers' wing spans.

Statistical Comparisons

As an initial cut, data for all aircraft, flowfield conditions and sensor elevation angles (2400 data points) are grouped together for each metric, with the statistical results for each of the 2 analytical procedures shown in Figure 7 and Figure 8. Generally, the results indicate weak relationships between aircraft response and metric values. Coefficient of Determination values are less than half of that indicating a good fit, and although Normalized Standard Deviation does not have a specific ideal value, most of the values are nearly an order of magnitude greater that those found in subsequent data reduction. Neither of the statistical indicators is explicitly tied to the *size* of the data set; rather, the poor results indicate that no single strength metric *relationship* can be reasonably used for all following aircraft and flowfield conditions. However, several trends in relative metric quality are evident, the most apparent being that the various flat-plate average circulation and roll moment selections perform similarly, while all of the gradient metrics show significantly weaker correlation. More specifically, trends indicate that gradient metric performance increases as observations are made closer to a given vortex. Also, it appears that smaller values of ΔR are preferable for near-vortex measurements, whereas larger ΔR values are favored when observations are made closer to the midpoint of the vortex pair. However, further analysis is required for an acceptable strength metric choice to emerge.

Another perspective is gained by subdividing the data into groups corresponding to each of the 10 following aircraft and 12 combinations of wake geometry parameters (i.e. 120 subsets of 20 values each). For each subset, comprised of data corresponding to the 10 leading aircraft and 2 different sensor elevation angles, quality (Coefficient of Determination, Normalized Standard Deviation) is computed for all metrics; they are then assigned a score using Eq. (21) based on their relative performance. The average results of these individual sub-analyses are given in Figure 9 and Figure 10, applying the constant-spacing and fixed-disturbance techniques respectively. The general quality of fit shows significant improvement because statistical relationships are determined for individual data subsets rather than processing all data concurrently. As shown in the figures, the average scores do not decrease monotonically with descending order of preference. This is because a candidate could rank above (or below) another in only a few individual cases, but by sufficient margins to achieve a greater (or lower) average quality rating. Still, the prevailing trend in average scores is mostly consistent with overall metric quality, indicating that metric performance is fairly robust with respect to variation in the wake characteristics and the encountering aircraft. Despite its statistical advantages, however, this data reduction technique does not offer a practical solution. There is almost complete disagreement between the constant-spacing and fixed-disturbance investigations in terms of metric preference. Furthermore, a consistently good *quality* of fit does not ensure that a metric would use the same relationship to predict values for all combinations of wake parameters and following aircraft; a set of strength metric functions covering all possible conditions would be excessive.

As a compromise between the first two cuts, data is partitioned such that analyses are performed for each individual following aircraft in *all* combinations of flowfield settings (i.e. 10 subsets of 240 values each). The average quality ratings and scores for these 10 cases are shown in Figure 11 and Figure 12. Overall, metric quality remains high; most of the Coefficients of Determination remain above 0.9, and the Normalized Standard Deviation values are less than double the previous values. Also, there is much greater correspondence between metric rankings obtained under constant-spacing and fixed disturbance assumptions. In previous research, when only considering relatively large following aircraft and strong wakes it was determined that the "C5-10" metric was the best choice for predicting aircraft response [Hinton and Tatnall 1997, 17]. However, the results here indicate that "C3-10" is the best overall choice for the full range of aircraft sizes and wake strengths, considering both average quality and average score

values. Of the roll moment metrics, the best overall choice is "H30tr0.7", although the average circulation metrics appear to offer generally better performance.

It can also be observed that the trend in average score is fairly sporadic for both methodologies, showing a significant variation in relative metric performance with type of following aircraft. This suggests the possibility of improved prediction capability with a class-based system of metrics determined by some property of the following aircraft. Also, further efforts to refine these metrics could benefit from knowledge of direct relationships between characteristics of the metrics and encountering aircraft.

Dependence on Aircraft Wing Span

Wing span is selected as the aircraft property for comparison purposes mainly because of its strong relationship to the induced loads which cause the aircraft disturbance. Additionally, span has the advantage of being a fixed value for each aircraft type, whereas mass-based quantities (i.e. weight and mass moment-of-inertia) are unpredictable due to varying amounts of fuel, cargo and/or passengers. Because the average quality values of the most preferable circulation and roll moment metrics are nearly identical, the top 3 metrics of each type in each of the two methodologies are selected for study in order to more completely represent trends. Due to consistently poor performance, the velocity gradient metrics are excluded from further study.

The first comparisons are made between wing span values and the averaging limits (r_a, r_b) of the three best flat-plate average circulation metrics for each individual analysis, as shown in Figure 13 and Figure 14. It appears that both inner and outer limits decrease with shorter follower wing span, particularly for values of $b_F < 30$ m. Also, there is a general decrease in the averaging limits for the fixed-disturbance cases. The plots confirm that "C3-10" would be the optimal choice for a *single* metric system. However, trends indicate that assigning different metrics to given ranges of following aircraft could improve results. Based on the limited pool of aircraft and averaging radius combinations, a *3-class* system emerges wherein "C3-10" is used when $b_F > 30$ m, "C1-10" when $15 \text{ m} < b_F \leqq 30$ m, and "C1-5" when $b_F \leqq 15$ m. It should also be observed that the averaging limits also decrease with wake strength, suggesting that the "C5-10" metric would not necessarily be the optimum choice even if smaller aircraft are ignored.

Similar comparisons are made between follower span and plate span used in the flat-plate roll moment metrics, as presented in Figure 15 and Figure 16. The values of optimal plate span generally decrease with follower wing span, which is expected since this basic metric model is designed to represent the roll moment induced on a follower's wing. In the same respect, however, it is surprising that almost all of the top-ranking roll moment metrics use a taper ratio of 0.7 despite the fact the most of the following aircraft have taper ratios around 0.3 and the highest values are around 0.5. While it would be reasonable to select "H30tr0.7" for use in a *single* metric system, patterns indicate that *2-class* system, in which "H30tr0.7" is used for $b_F > 20$ m and "H15tr0.7" for $b_F \leqq 20$ m, could offer better results.

To further investigate relationships between wing span and the optimal radial averaging limits used in the flat-plate average circulation metric (r_a, r_b), these values are plotted are plotted as fractions of follower wing span in Figure 17 and Figure 18. The inner radius values appear to fluctuate around roughly 10% of the follower's wing span; although harder to distinguish due to the limited number of possible choices, the outer radius values range from around 20-60%, but seem to center on 30-40% of the follower's span. Similarly, the ratios of plate spans (B) to follower wing span are plotted in Figure 19 and Figure 20. Both figures indicate a direct correspondence between follower wing span and plate span.

5. CONCLUSIONS

Candidate wake vortex strength metrics, based on a series of velocity measurements taken by an idealized fixed ground sensor, are evaluated and rated based on their ability to predict the amount of roll disturbance experienced by an aircraft encountering a given flowfield. Aircraft response and metric reading data are computed for a variety of aircraft, flowfield, and sensor conditions. In response to concerns that a given metric may not accurately predict aircraft roll disturbance for all ranges of wake strength, parallel investigations are performed in which either the aircraft separation distance is held constant or the disturbance angle is fixed at fairly low value. Metrics are then rated according to either how well their values linearly correlate to computed roll angles, or how precisely they produce a given value for the prescribed disturbance angle, respectively.

From the list of possible candidates for flat-plate average circulation and roll moment metrics, selections are made for both single-metric and class-based systems, as shown in Table 5. Although these selections perform consistently better than the others, most of the average circulation and roll moment metrics perform well enough that there is some latitude in altering the final specifications (r_a, r_b, B) to meet other criteria, such as sensor limitations. Overall, average circulation appears to be more advantageous than roll moment: the average circulation metrics show generally superior performance, and the roll moment concept introduces the additional uncertainty of selecting an appropriate plate taper ratio. The velocity gradient metrics did not show good correlation with aircraft response data based on the limited number of cases, and thus were not included in the final analysis.

TABLE 5

SUMMARY OF RECOMMENDED STRENGTH METRIC SELECTIONS

	Flat-Plate Avg. Circulation	Flat-Plate Roll Moment
Single Metric System	C3-10	H30tr0.7
Class-Based System	$b_F > 30$ m : C3-10 30 m $\geqq b_F > 15$ m : C1-10 $b_F \leqq 15$ m : C1-5	$b_F > 20$ m : H30tr0.7 $b_F \leqq 20$ m : H15tr0.7

Using the models and tools developed herein, further research can be conducted in the following areas:

- Generate roll response data (and corresponding metric values) for additional wake conditions, such as tilted vortex pairs, or using image vortices to simulate ground effects; include additional aircraft, particularly small following aircraft which face the greatest threat, or aircraft with unique wing spans which could "fill in the gaps" left by the current limited population.
- Perform calculations for various wake strengths (i.e. different aircraft separations), and determine non-linear relationships that maintain accuracy over all ranges of roll response values.
- Consider additional variations of the flat-plate average circulation and roll moment concepts, particularly using characteristics which could clarify relationships with follower wing span.

Beyond the given models and assumptions, future study could include higher-fidelity aircraft dynamic response models, or a more involved measure of aircraft threat than simply roll disturbance angle. Also, sensor-specific traits and limitations will ultimately play a role in selecting a final strength metric definition for the AVOSS.

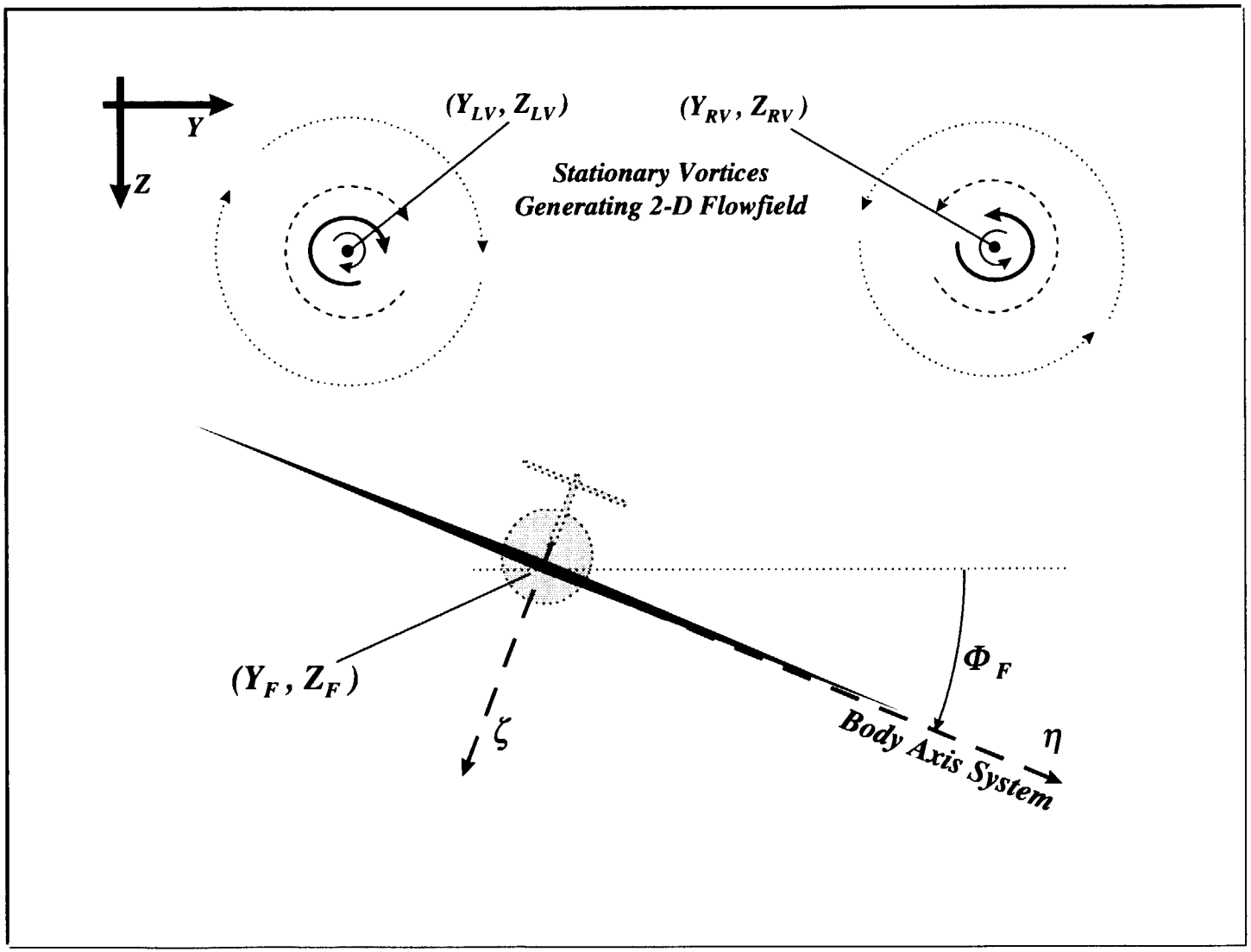

Figure 1. Illustration of method and assumptions used in computing vortex-induced aircraft response.

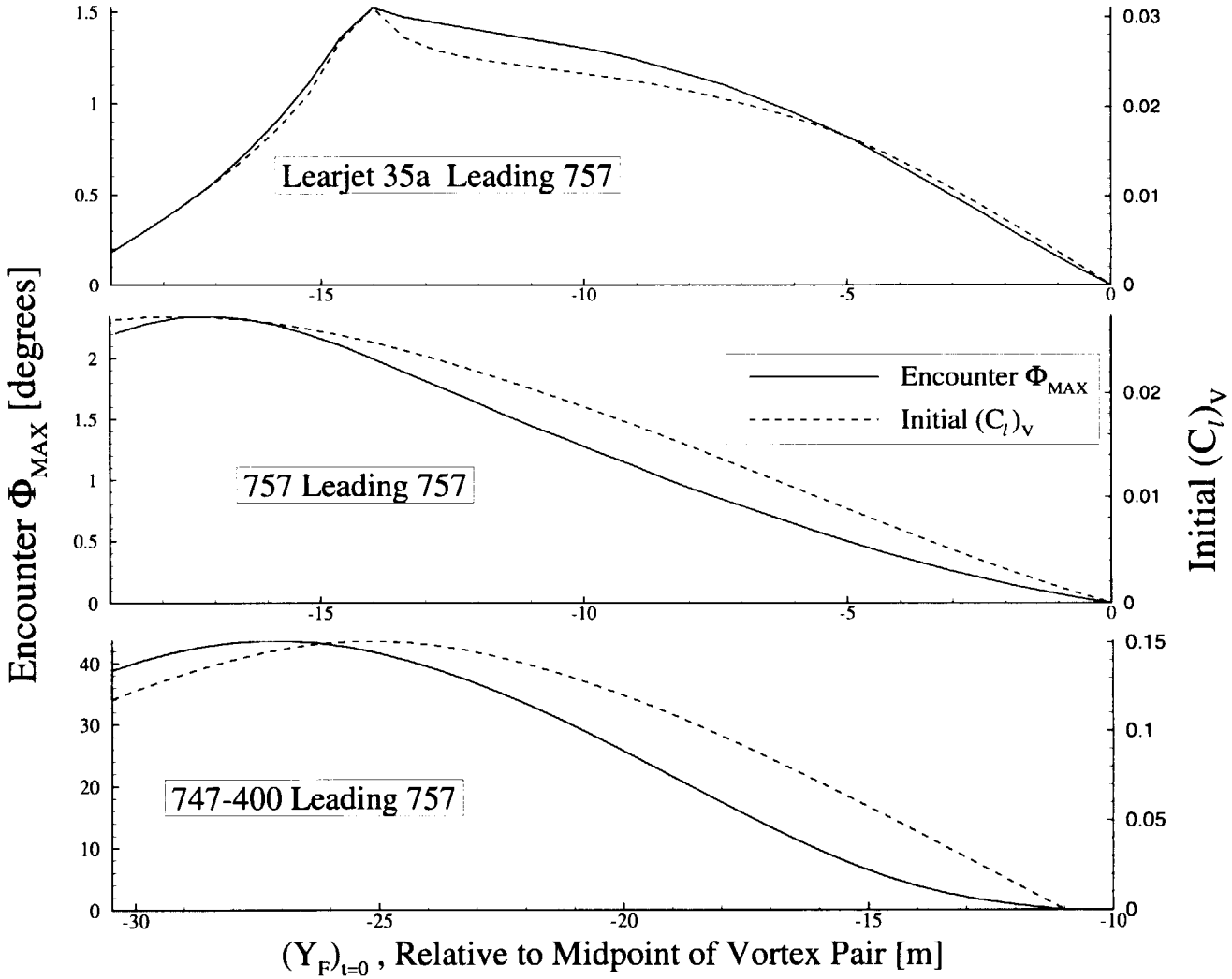

Figure 2. Comparisons of trends in maximum encounter roll disturbance and induced roll moment for Boeing 757 following three different aircraft, assuming r_C = 0.2% b_G, vortices separated $\pi/4$ b_G, and aircraft separated 3 nm.

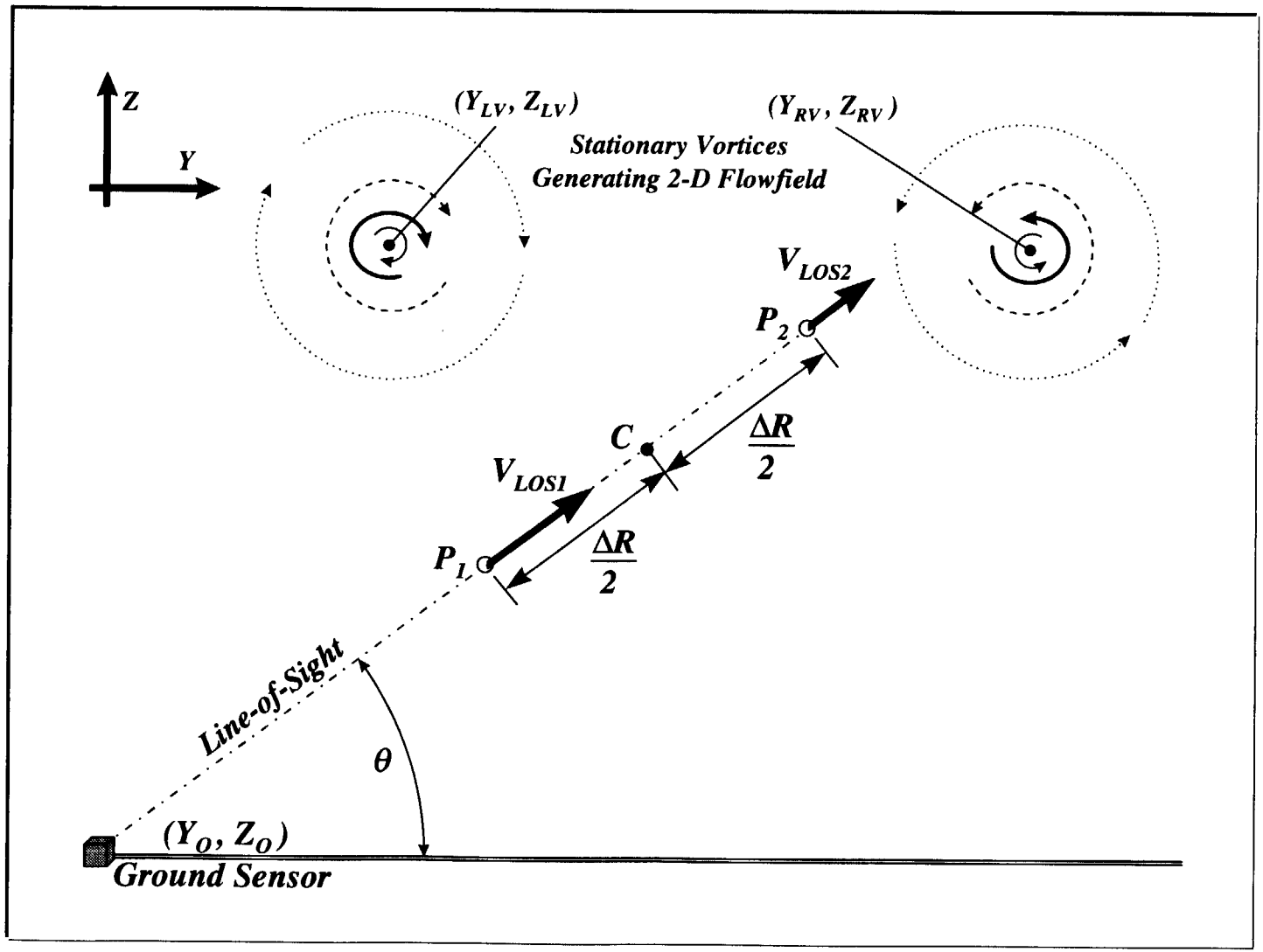

Figure 3. Illustration of the Velocity Gradient Metric concept.

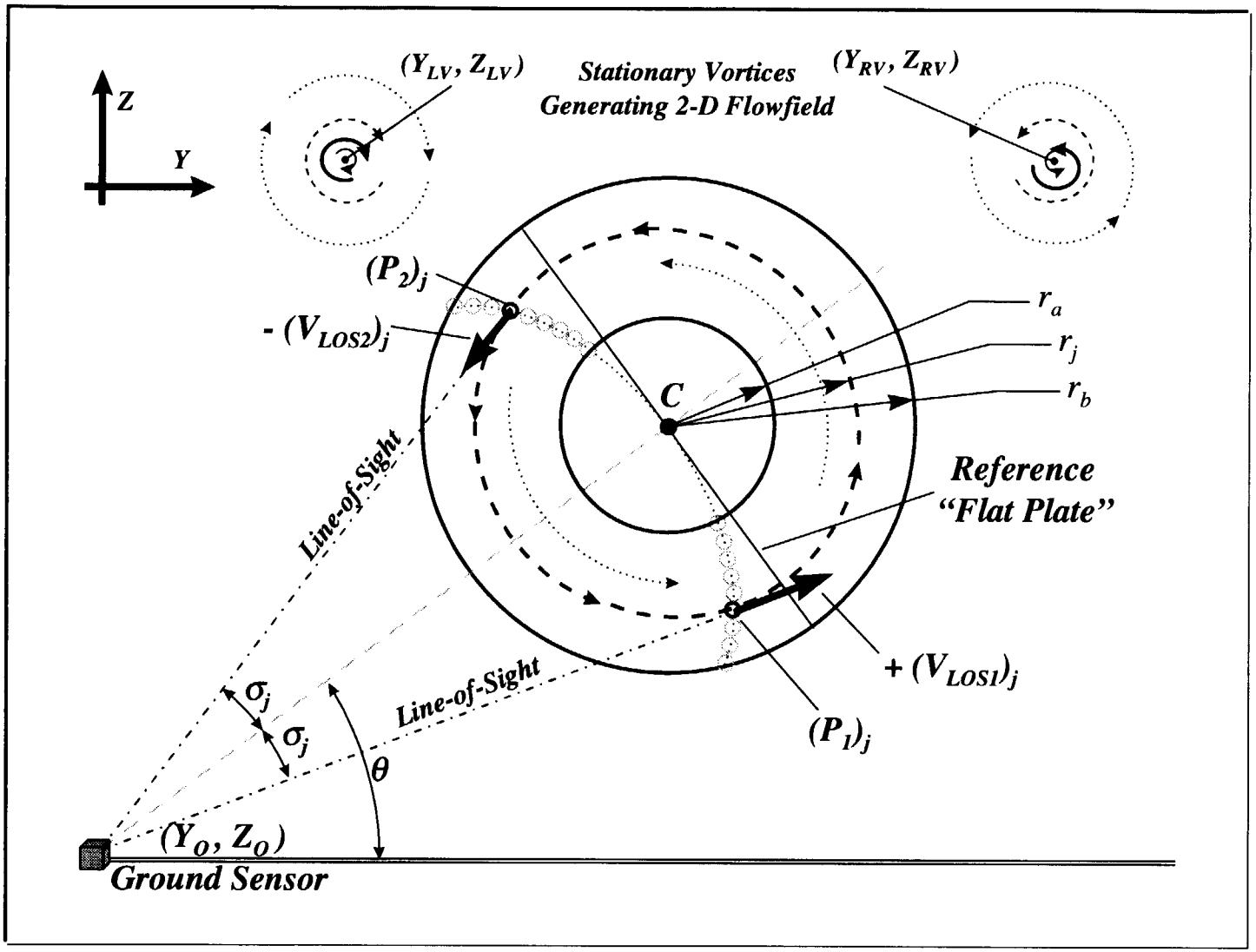

Figure 4. Illustration of the Flat-Plate Average Circulation Metric concept.

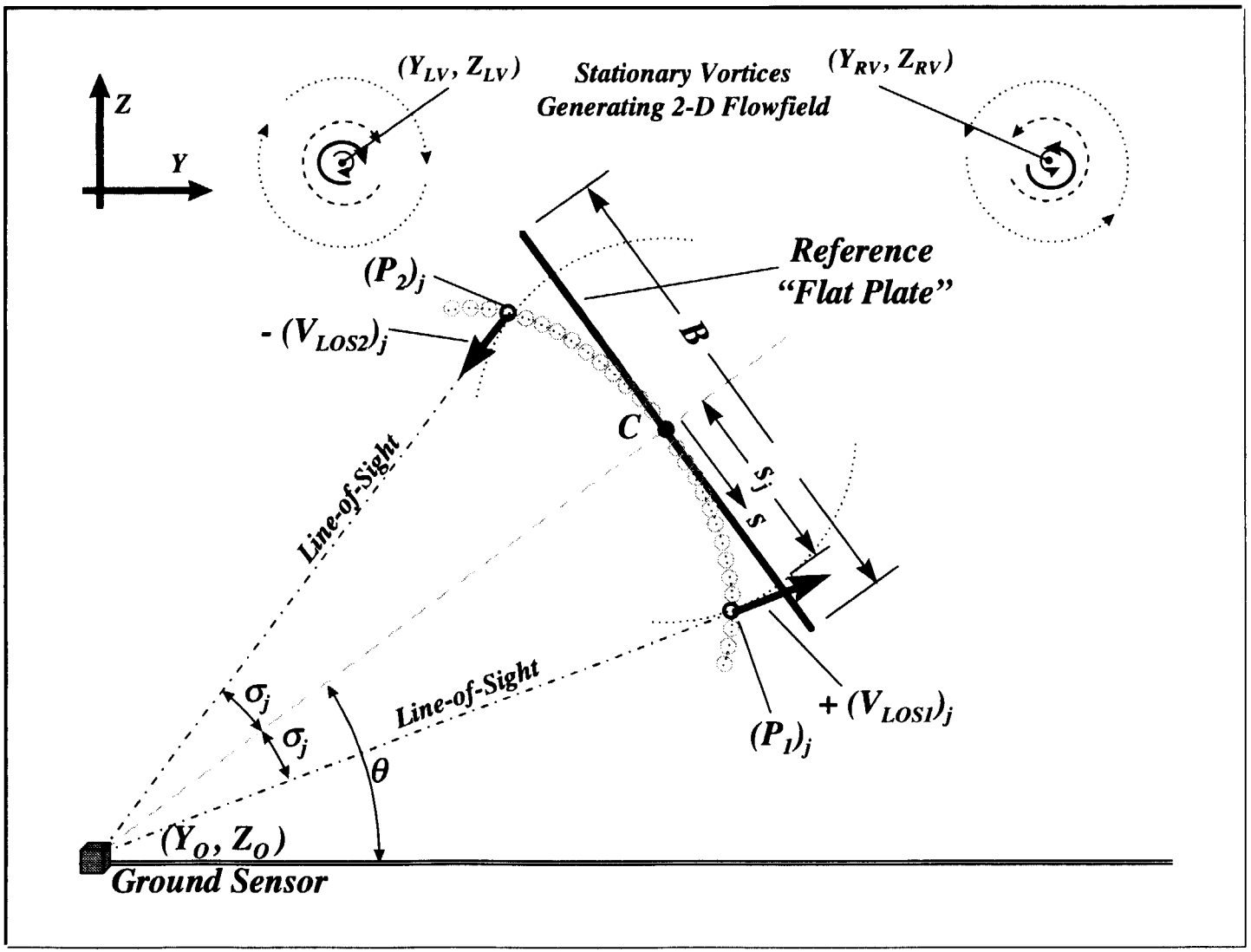

Figure 5. Illustration of the Flat-Plate Roll Moment Metric concept.

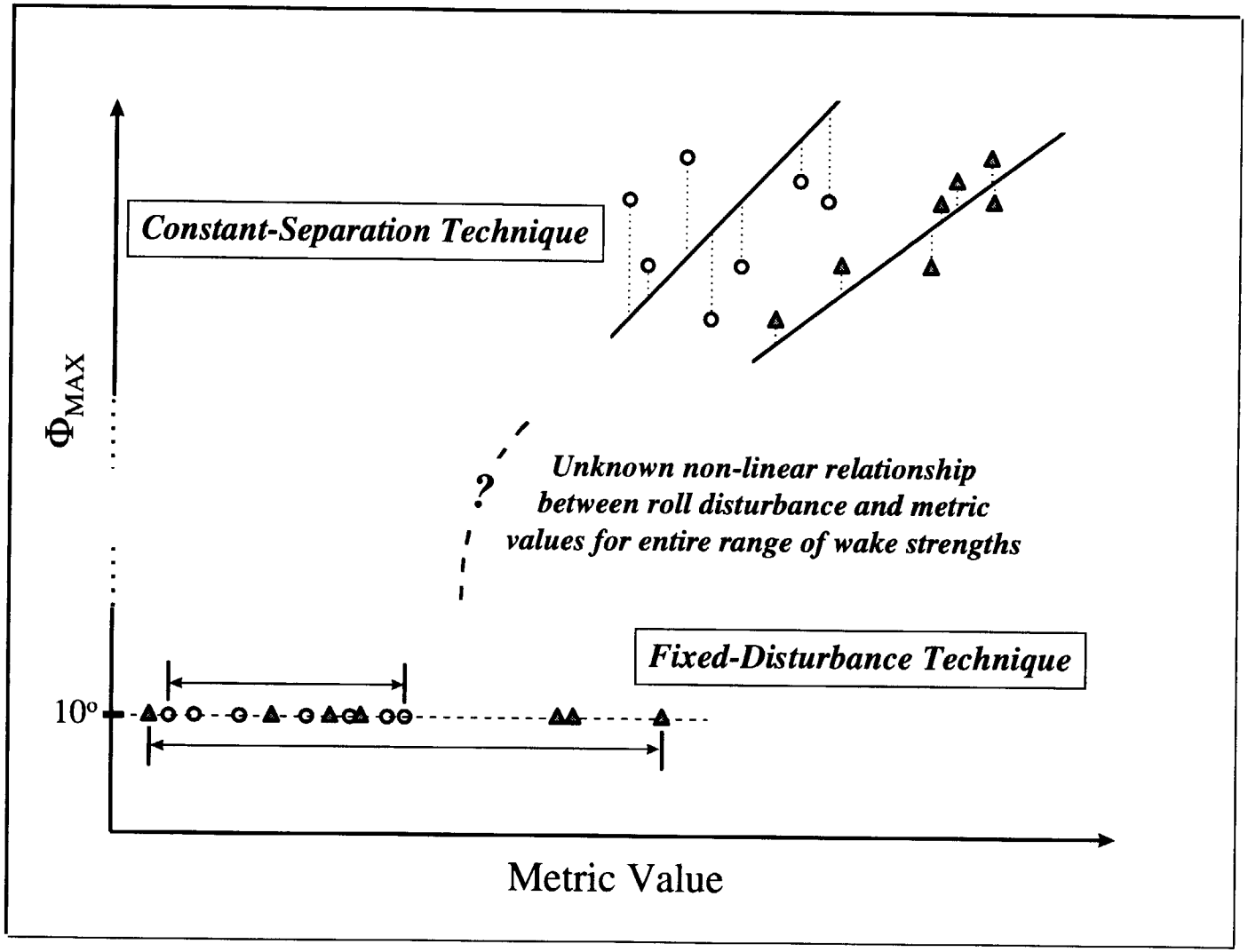

Figure 6. Representation of different approaches taken to evaluate and compare candidate metrics. In this example, the metric corresponding to the triangle symbols is superior in predicting only larger disturbance values.

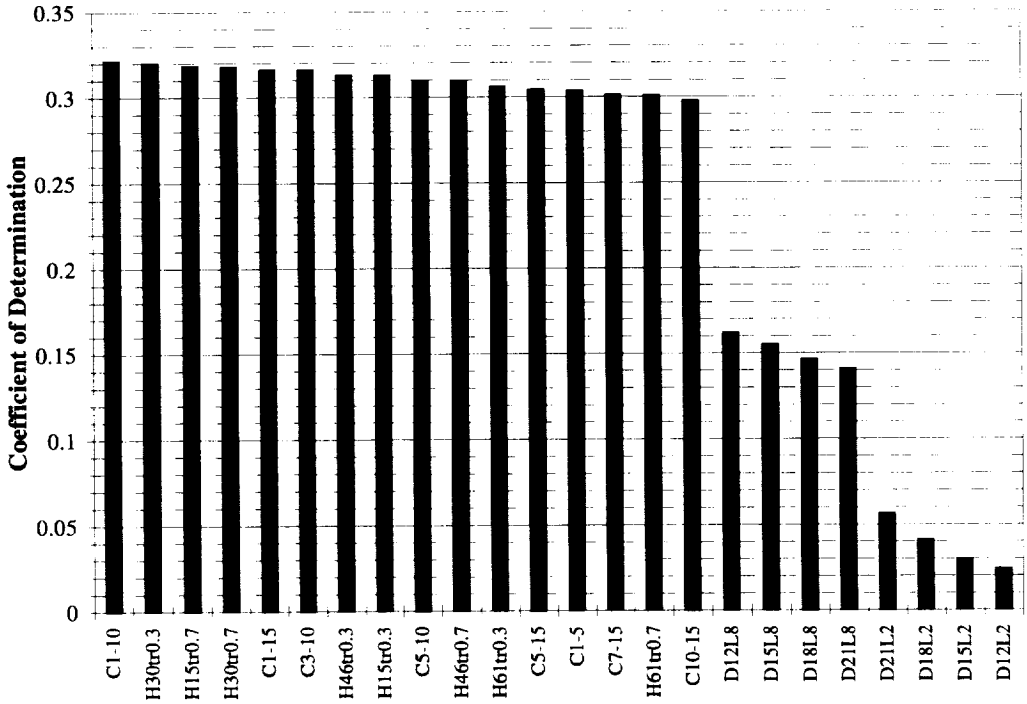

Figure 7. Metrics sorted in order of preference, using the constant-spacing methodology and performing regression with all data for each metric.

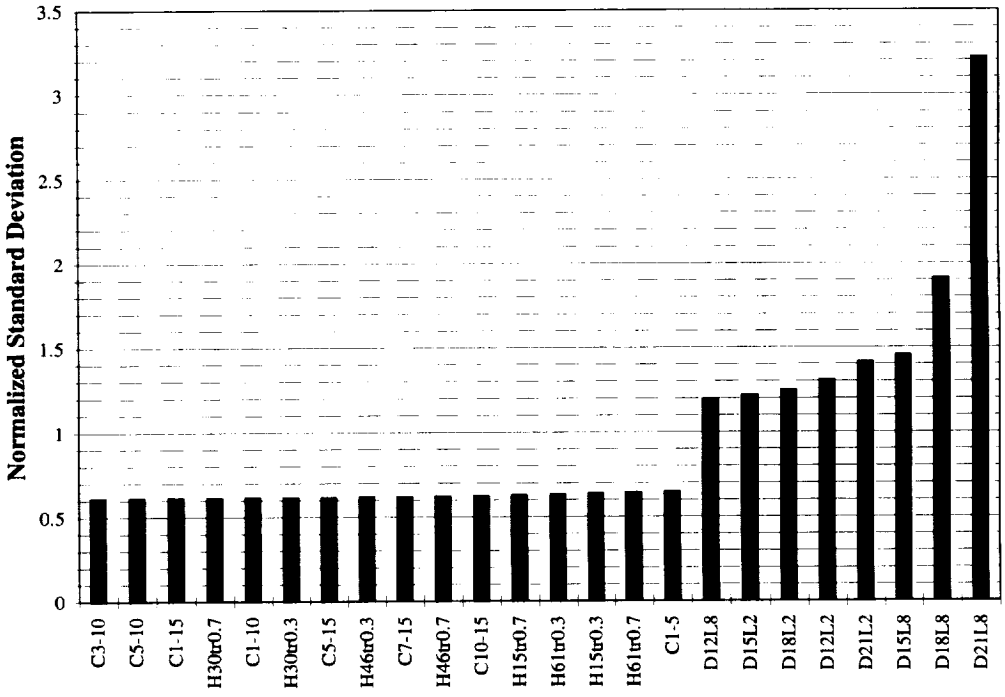

Figure 8. Metrics sorted in order of preference, using the fixed-disturbance methodology and computing mean and standard deviation of all data for each metric.

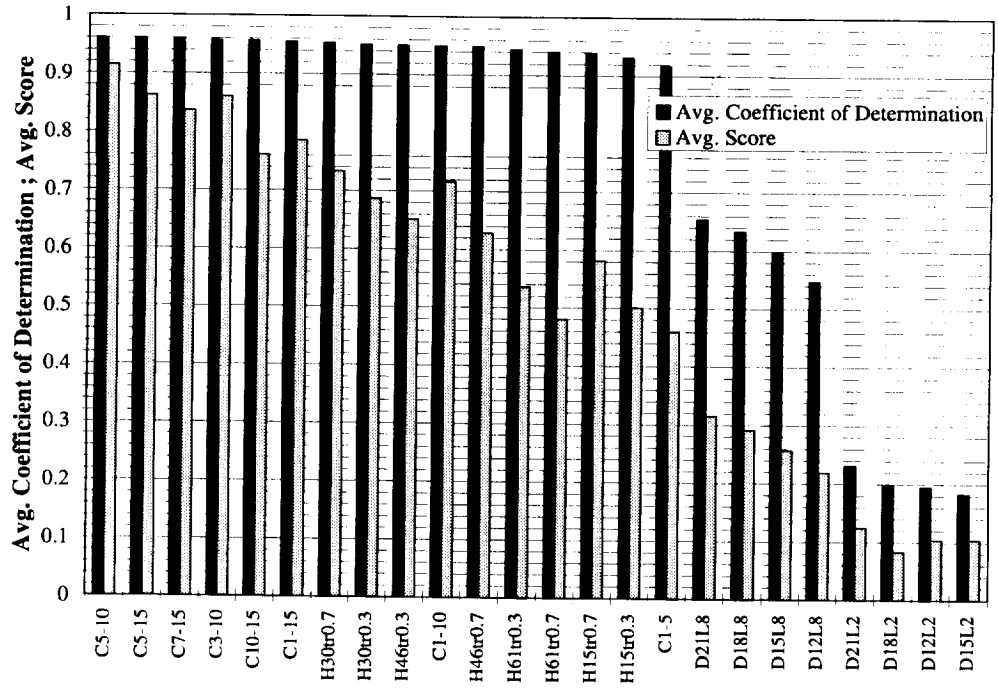

Figure 9. Metrics sorted in order of preference given with average relative scores, based on the constant-spacing methodology. Regression is performed separately for each combination of follower and wake parameters.

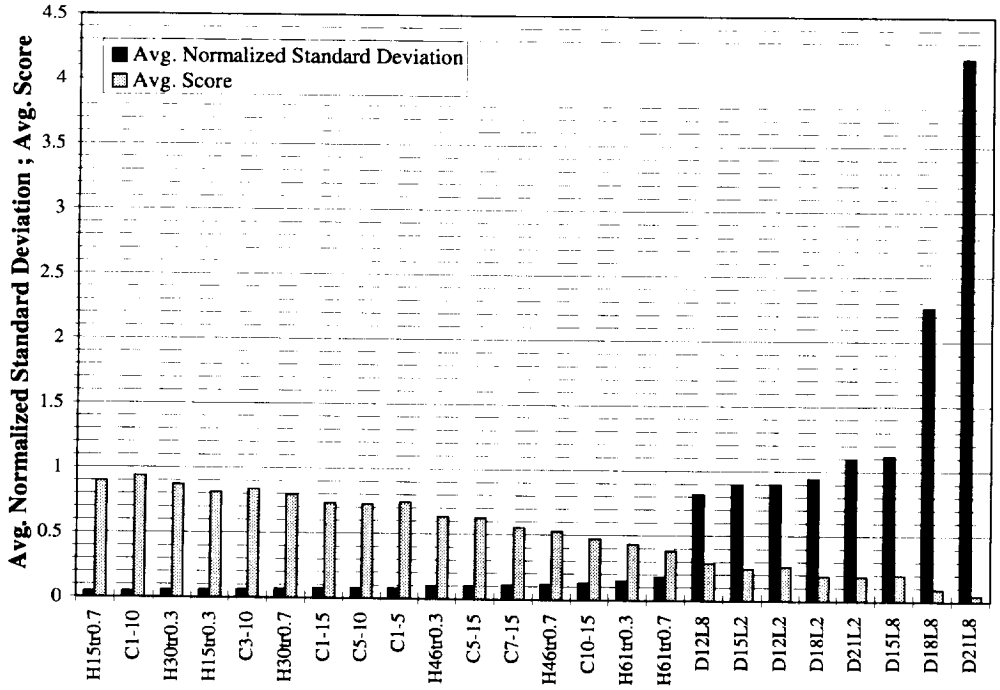

Figure 10. Metrics sorted in order of preference given with average relative scores, based on the fixed-disturbance methodology. Statistical computations are performed separately for each combination of follower and wake parameters.

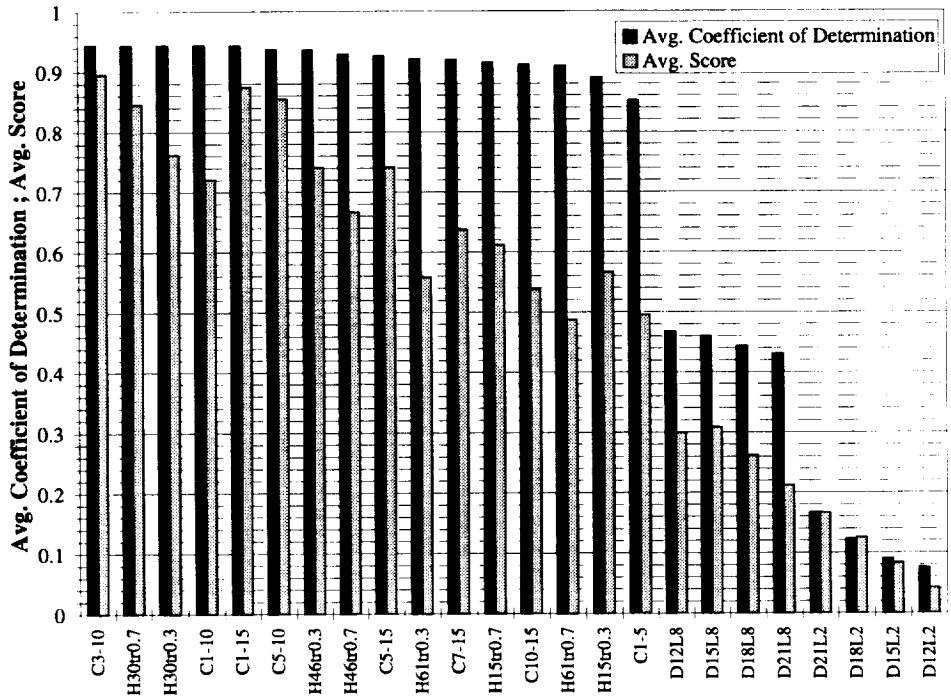

Figure 11. Metrics sorted in order of preference along with average relative scores, based on the constant-spacing methodology. Regression is performed using all combinations of wake parameters for each individual follower.

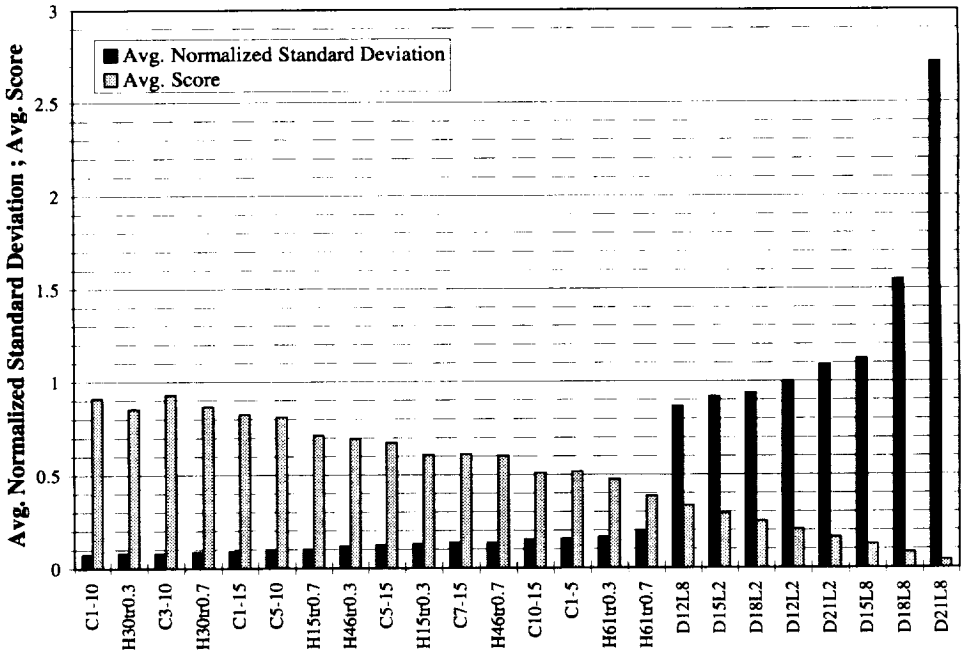

Figure 12. Metrics sorted in order of preference given with average relative scores, based on the fixed-disturbance methodology. Statistical computations are performed using all combinations of wake parameters for each individual follower.

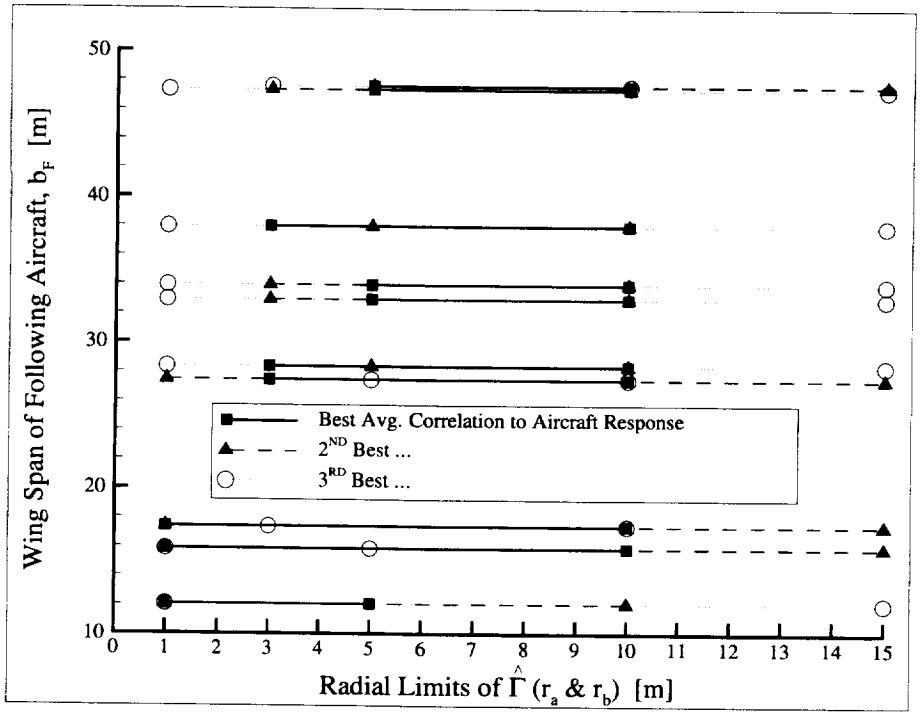

Figure 13. Averaging limits of the three most effective flat-plate average circulation metrics plotted against wing spans of the associated followers, using the constant-spacing methodology.

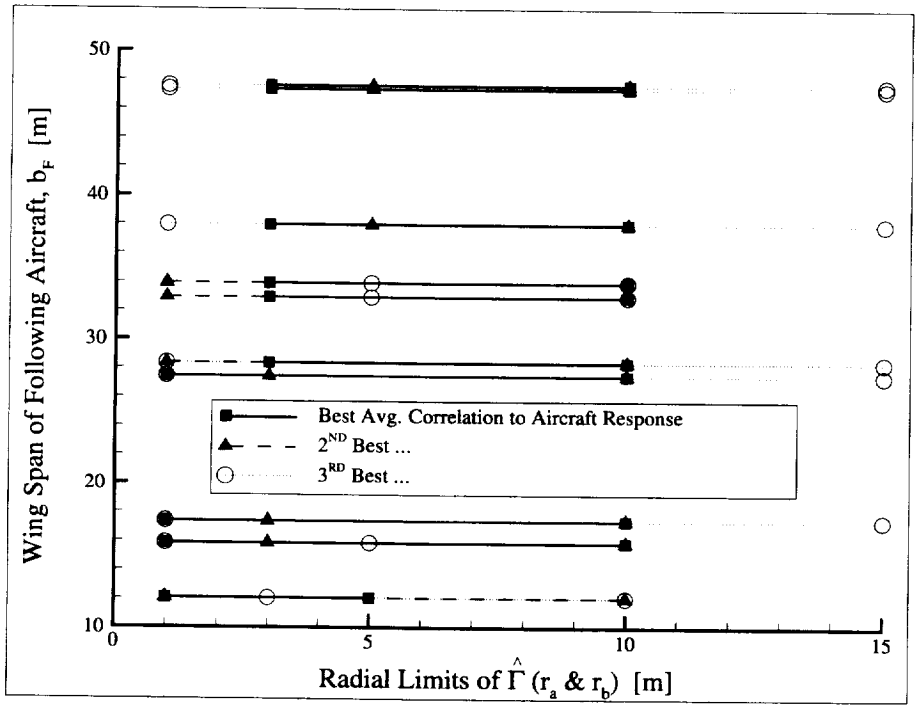

Figure 14. Averaging limits of the three most effective flat-plate average circulation metrics plotted against wing spans of the associated followers, using the fixed-disturbance methodology.

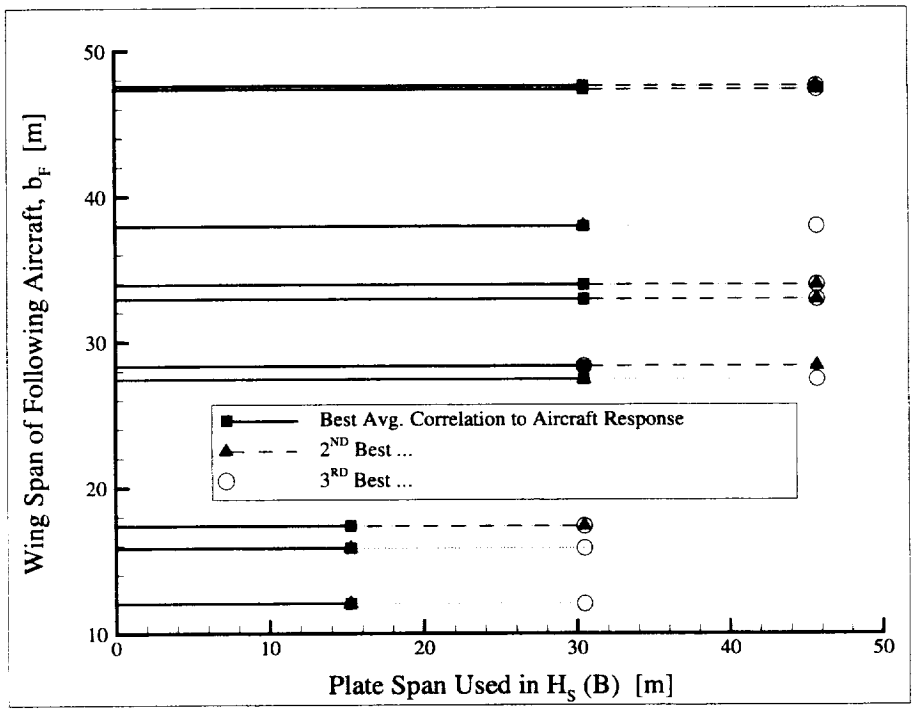

Figure 15. Plate span lengths of the three most effective flat-plate roll moment metrics plotted against wing spans of the associated followers, using the constant-spacing methodology.

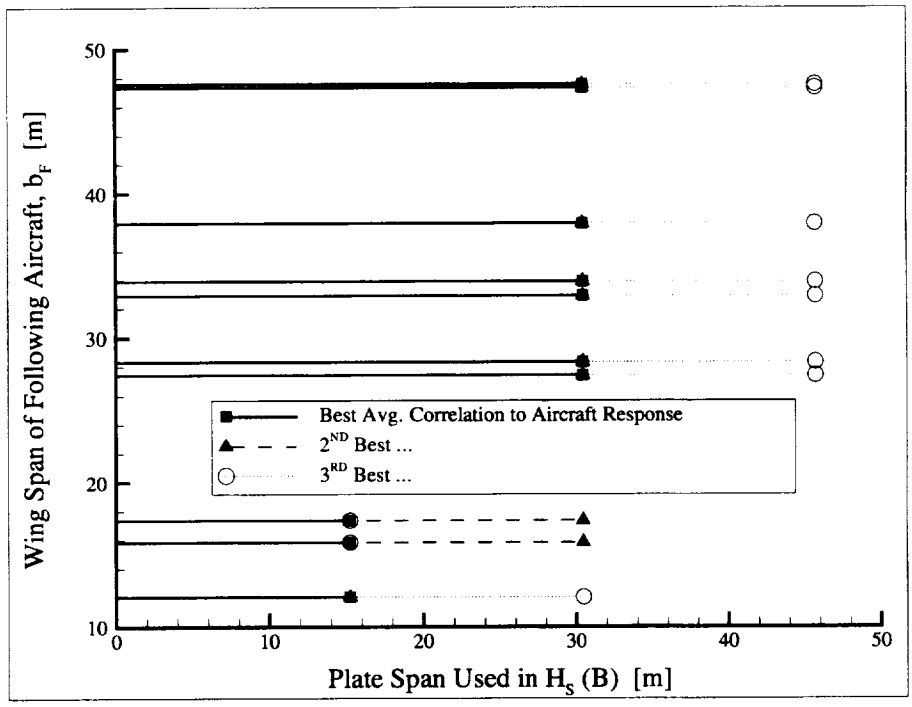

Figure 16. Plate span lengths of the three most effective flat-plate roll moment metrics plotted against wing spans of the associated followers, using the fixed-disturbance methodology.

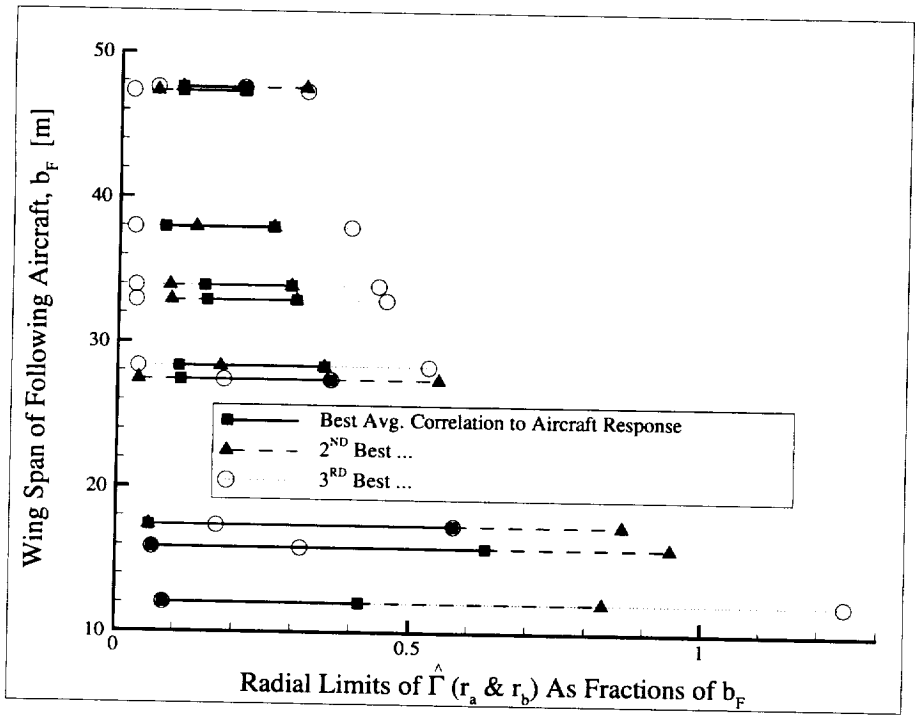

Figure 17. Ratios of averaging limits to associated followers' wing spans for the three most effective flat-plate average circulation metrics plotted against corresponding spans, using the constant-spacing methodology.

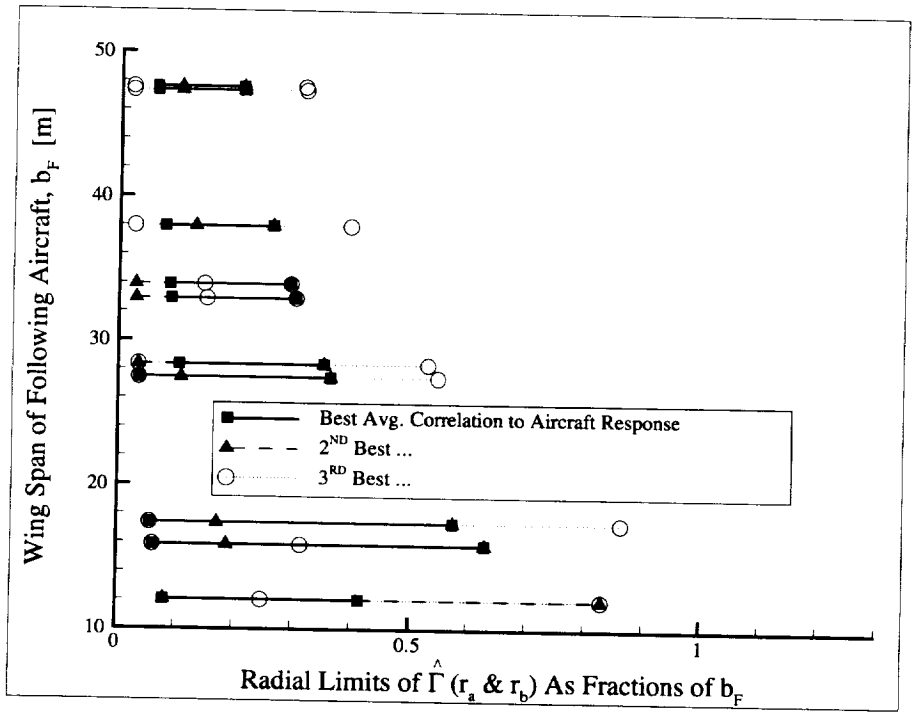

Figure 18. Ratios of averaging limits to associated followers' wing spans for the three most effective flat-plate average circulation metrics plotted against corresponding spans, using the fixed-disturbance methodology.

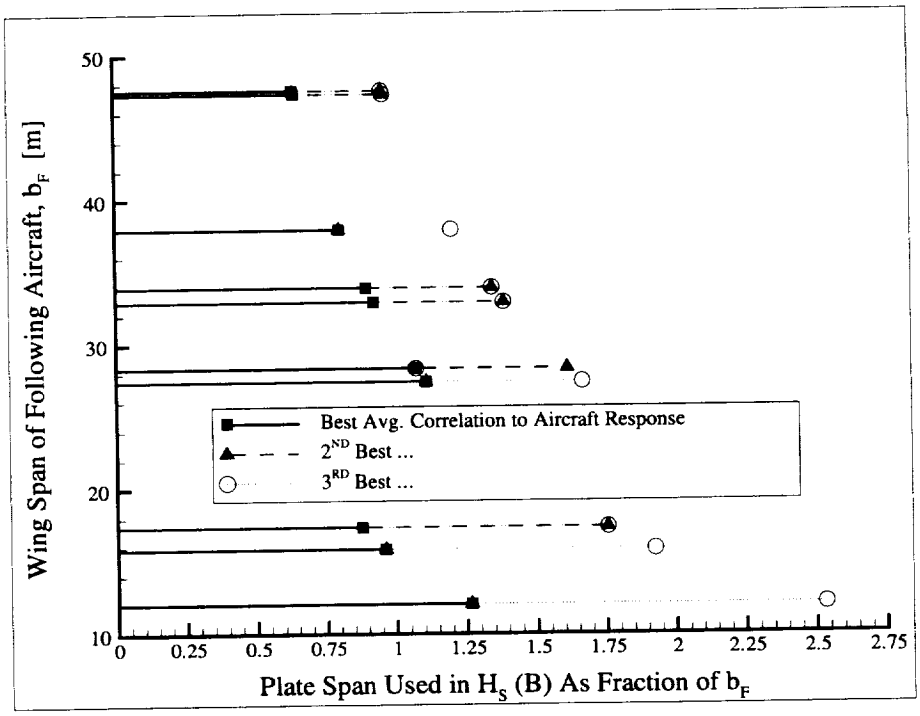

Figure 19. Ratios of plate span lengths to associated followers' wing spans for the three most effective flat-plate roll moment metrics plotted against corresponding spans, using the constant-spacing methodology.

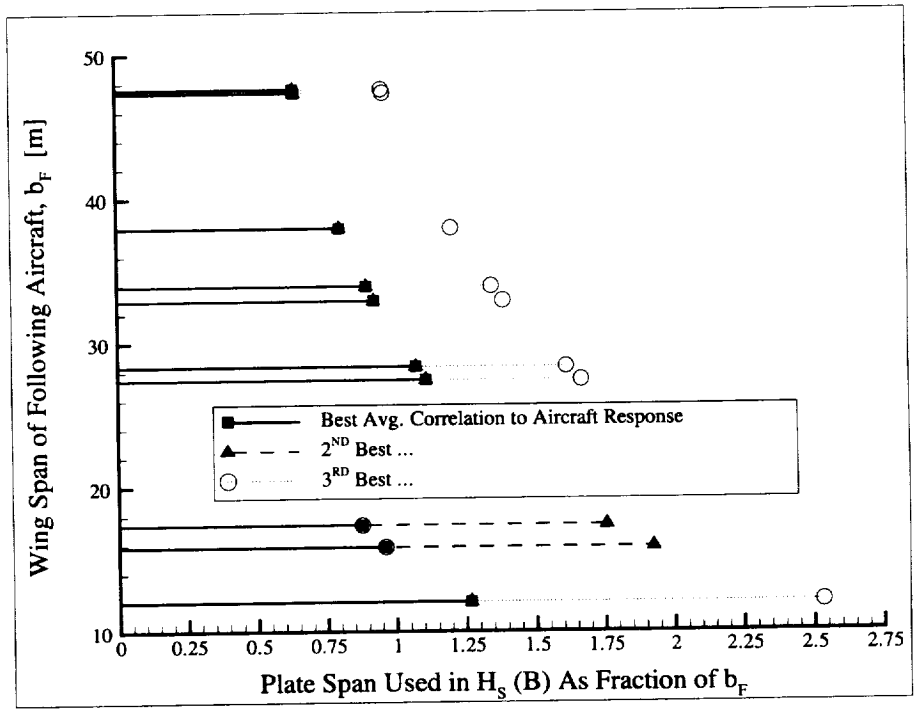

Figure 20. Ratios of plate span lengths to associated followers' wing spans for the three most effective flat-plate roll moment metrics plotted against corresponding spans, using the fixed-disturbance methodology.

REFERENCES

Burnham, D. C., and Hallock, J. N. 1982. Chicago Monostatic Acoustic Vortex Sensing System. Vol. 4, Wake Vortex Decay. Springfield, VA: National Technical Information Service.

Critchley, J. B., and Foot, P. B. 1991. United Kingdom Civil Aviation Authority Database: Analysis of Incidents Reported Between 1972 and 1990" In Proceedings of the Aircraft Wake Vortices Conference, Washington, DC, October 29-31, 1991, Vol. 1, by the National Technical Information Service. Springfield, VA: National Technical Information Service.

Hallock, J. N. 1991. Aircraft Wake Vortices: An Assessment of the Current Situation. Cambridge, MA: U.S. Department of Transportation, Research and Special Programs Administration. DOT-FAA-RD-90-29.

Hinton, David A. 1995. Aircraft Vortex Spacing System (AVOSS) Conceptual Design. NASA Technical Memorandum 110184.

Hinton, David A., and Tatnall, Christopher R. 1997. A Candidate Wake Vortex Strength Definition for Application to the NASA Aircraft Vortex Spacing System (AVOSS). NASA Technical Memorandum 110343.

Johnson, Amanda. 1991. Trends in wake vortex incidents. In Proceedings of the Aircraft Wake Vortices Conference, Washington, DC, October 29-31, 1991, Vol. 1, by the National Technical Information Service. Springfield, VA: National Technical Information Service.

Karamcheti, Krishnamurty. 1980. Principles of Ideal-Fluid Aerodynamics. New York: Wiley, 1966; reprint, Malabar, FL: Krieger Publishing Co. (page references are to reprint edition).

Lamb, H. 1932. Hydrodynamics, 6th Ed. Cambridge University Press.

Saffman, P.G. 1992. Vortex Dynamics. Cambridge University Press.

Scheaffer, Richard L., and McClave, James T. 1986. Probability and Statistics for Engineers, 2nd Ed. Boston: Duxbury Press.

Scott, William B. Technology, Economics, Fuel, Public-Private Cooperation. Aviation Week & Space Technology, June 7, 1993.

Tatnall, Christopher R. 1995. A Proposed Methodology for Determining Wake-Vortex Imposed Aircraft Separation Constraints M.S. thesis, George Washington University.

Tinling, Bruce E. 1977. Estimation of Vortex-Induced Roll Excursions Based on Flight and Simulation Results. In Proceedings of the aircraft wake-vortices conference held at Kendall Square, Cambridge, MA, March 15-17, 1977, edited by J. N. Hallock.

U.S. Department of Transportation. Federal Aviation Administration. 1997. Air Traffic Control 7110.65K. [Washington, D.C.]: U. S. Department of Transportation, Federal Aviation Administration.

Vicroy, Dan; Bowles, Roland; Brandon, Jay; Greene, George; Jordan, Frank, Jr.; Rivers, Robert; Stewart, Eric; Stough, H. Paul, III and Stuever, Robert. 1994. NASA Wake Vortex Research. ICAS-94-6.2.2, 19th Congress of the International Council of the Aeronautical Sciences, Anaheim, CA, 19-23 September 1994.

Von Mises, R. 1959. Theory of Flight. New York: Dover Publications.

REPORT DOCUMENTATION PAGE

Form Approved OMB No. 0704-0188

1. AGENCY USE ONLY (*Leave blank*)	2. REPORT DATE	3. REPORT TYPE AND DATES COVERED
	March 1998	Contractor Report

4. TITLE AND SUBTITLE
An Investigation of Candidate Sensor-Observable Wake Vortex Strength Parameters for the NASA Aircraft Vortex Spacing System (AVOSS)

5. FUNDING NUMBERS
NCC1-24
538-04-11-11

6. AUTHOR(S)
Christopher R. Tatnall

7. PERFORMING ORGANIZATION NAME(S) AND ADDRESS(ES)
George Washington University
Joint Institute for Advancement of Flight Sciences
Langley Research Center
Hampton, VA 23681-2199

8. PERFORMING ORGANIZATION REPORT NUMBER

9. SPONSORING/MONITORING AGENCY NAME(S) AND ADDRESS(ES)
National Aeronautics and Space Administration
Langley Research Center
Hampton, VA 23681-2199

10. SPONSORING/MONITORING AGENCY REPORT NUMBER
NASA/CR-1998-206933

11. SUPPLEMENTARY NOTES
A Professional Degree Project submitted to the faculty of The School of Engineering and Applied Science of The George Washington University in partial satisfaction of the requirements for the degree of Professional Engineer. Langley Technical Monitor: David Hinton.

12a. DISTRIBUTION/AVAILABILITY STATEMENT
Unclassified-Unlimited
Subject Category 03 Distribution: Standard
Availability: NASA CASI (301) 621-0390

12b. DISTRIBUTION CODE

13. ABSTRACT (*Maximum 200 words*)
The counter-rotating pair of wake vortices shed by flying aircraft can pose a threat to ensuing aircraft, particularly on landing approach. To allow adequate time for the vortices to disperse/decay, landing aircraft are required to maintain certain fixed separation distances. The Aircraft Vortex Spacing System (AVOSS), under development at NASA, is designed to prescribe safe aircraft landing approach separation distances appropriate to the ambient weather conditions. A key component of the AVOSS is a ground sensor, to ensure safety by making wake observations to verify predicted behavior. This task requires knowledge of a flowfield strength metric which gauges the severity of disturbance an encountering aircraft could potentially experience. Several proposed strength metric concepts are defined and evaluated for various combinations of metric parameters and sensor line-of-sight elevation angles. Representative populations of generating and following aircraft types are selected, and their associated wake flowfields are modeled using various wake geometry definitions. Strength metric candidates are then rated and compared based on the correspondence of their computed values to associated aircraft response values, using basic statistical analyses.

14. SUBJECT TERMS
wake vortex; aviation safety; airport operations; aircraft stability and control; wake vortex sensing

15. NUMBER OF PAGES
42

16. PRICE CODE
A03

17. SECURITY CLASSIFICATION OF REPORT	18. SECURITY CLASSIFICATION OF THIS PAGE	19. SECURITY CLASSIFICATION OF ABSTRACT	20. LIMITATION OF ABSTRACT
Unclassified	Unclassified	Unclassified	

NSN 7540-01-280-5500

Standard Form 298 (Rev. 2-89)
Prescribed by ANSI Std. Z-39-18
298-102